2019-02-15

Coastal embayment rotation: Response to extreme events and climate control, using full embayment surveys

Wiggins, Mark

10.1016/j.geomorph.2018.11.014
Geomorphology
Elsevier

Geomorphology 327 (2019) 385–403

Contents lists available at ScienceDirect

Geomorphology

journal homepage: www.elsevier.com/locate/geomorph

Invited research article

Coastal embayment rotation: Response to extreme events and climate control, using full embayment surveys

Mark Wiggins *, Tim Scott, Gerd Masselink, Paul Russell, Robert Jak McCarroll

Coastal Processes Research Group, School of Biological and Marine Sciences, University of Plymouth, Plymouth, UK

ARTICLE INFO

Article history:
Received 6 July 2018
Received in revised form 12 November 2018
Accepted 13 November 2018
Available online 19 November 2018

Keywords:
Storm response
Beach morphodynamics
Sediment budget
Headland bypassing
Beach rotation

ABSTRACT

Barrier beach change in directionally bi-modal wave climates presents an increasing challenge for coastal communities, both in the short-term (storm events), and decadal to centurial time scales (long-term evolution). Predicting and planning for subsequent variations requires understanding of the morphological response to changes in wave energy, along with the atmospheric forces driving the wave climate. In this paper, multi-method topo-bathymetric surveys are used to assess the morphological change of a semi-sheltered gravel barrier (Start Bay, Devon, UK). Total sediment budgets (supra- to sub-tidal), with spatially-varying uncertainty levels, indicate the embayment is closed. One third of total sediment flux occurred in the sub-tidal, establishing the importance of sub-tidal transport for this type of coastline. Our results demonstrate that under the predominance of a given wave direction, rotation first occurs within sub-embayments. Additional sustained and extreme energy levels are then required for full embayment rotation to occur, with significant headland bypassing. In this instance, 6×10^5 m^3 of gravel was transported alongshore during a 3-year sustained period of dominant-southerly waves, including a 1:50 year storm season (full-embayment rotation), whilst 3×10^5 m^3 was returned during a 2-year period of dominant easterly waves (sub-embayment rotation only). A novel parameter is introduced that predicts beach rotation based on the directional wave balance. In turn, winter wave direction is shown to correlate with a combination of two climate indices. Given adequate predictions of relevant climate indices, these findings constitute the basis of a generalisable method to predict and plan for future beach rotation on similar beaches globally.

1. Introduction

Gravel barrier beaches often act as the first line of defense from elevated water levels and wave forcing during storms, absorbing wave energy at the shoreline and providing protection from inundation for housing and infrastructure (Poate et al., 2016). These mobile barrier deposits are highly dynamic and respond rapidly to changes in wave climate (Ruiz de Alegria-Arzaburu and Masselink, 2010; Bergillos et al., 2016a; Bergillos et al., 2017). Therefore, effective planning and management of gravel coasts requires a comprehensive understanding of the morphological response to changes in the incoming wave climate over a range of different timescales. Extreme storm events can rapidly reduce beach volumes, often resulting in coastal inundation and impacting coastal vulnerability (Santos et al., 2017). Annual to multi-decadal variations in both the incident wave height and dominant wave direction, can drive subtle but cumulatively substantial changes to beach planform and profile shape (Ranasinghe et al., 2004; Harley et al., 2017), leaving coastal communities at risk of erosion and flooding, highlighting the need for improved morphodynamic understanding and effective planning where future climate scenarios incorporate increased wave climate variability (Mortlock and Goodwin, 2016; van Maanen et al., 2016; Castelle et al., 2018).

For embayed beaches, where incident wave angles are oblique, morphological changes are often dominated by longshore transport processes, with sediment transported in the direction of wave approach (Short and Masselink, 1999). When directionally sustained, beaches erode and narrow at the up-drift extent and accrete and widen at the down-drift extent, with the subsequent change in planform orientation known as "rotation" (Klein et al., 2002). Beach rotation at some embayed beaches is also linked to variations in alongshore gradients in wave energy, resulting in increased or decreased cross-shore sediment exchange, leading to an out of phase response at embayment extremities (e.g. Harley et al., 2011). In contrast, where the incident wave climate is directionally bi-modal, morphological changes are often controlled by the time-integrated balance of wave power from the two directions (Ruiz de Alegria-Arzaburu and Masselink, 2010; Bergillos et al., 2016b).

Rotation-dominated embayments in directionally bi-modal wave climates are sensitive to extreme storm events from particular

* Corresponding author at: Reynolds Building, Drake Circus, Plymouth, Devon PL4 8AA, UK.
E-mail address: mark.wiggins@plymouth.ac.uk (M. Wiggins).

https://doi.org/10.1016/j.geomorph.2018.11.014

directions. Masselink et al. (2015) and Scott et al. (2016) observed significant south coast rotation following a series of southerly storms (see Section 2.2), where wave approach was oblique to the shoreline. The volumetric response was observed in detail at Slapton Sands (Start Bay, South Devon, UK), a semi-sheltered, embayed gravel barrier. Critically, Scott et al. (2016) identified that net inter-tidal volume change was negative between pre and post winter surveys, indicating sediment loss through either cross-shore processes (offshore transport and/or barrier over wash), or between sub-embayments via subaqueous headland bypassing (Ojeda and Guillén, 2008).

The lack of understanding of the fate of observed intertidal sediment losses in the alongshore (Harley et al., 2015; Burvingt et al., 2017), between sub-embayments (Thomas et al., 2010; Goodwin et al., 2013), and on/offshore (Davidson et al., 2013; Poate et al., 2015), limits the understanding of the mechanisms driving spatial and temporal morphological change, specifically beach recovery from extreme wave events (Corbella and Stretch, 2012; Scott et al., 2016; Burvingt et al., 2018). Robust calculations of total sediment budgets are difficult within the coastal zone and often only sub-aerial (e.g. Burvingt et al., 2016), or sub-tidal (e.g. Shaw et al., 2008) beach changes are assessed. The resultant temporal comparisons may lack consideration of uncertainty induced by the survey technique, sampling and interpolation, producing estimates of geomorphic volume change with limited confidence (Williams, 2012). Recent advances in fluvial geomorphology (Wheaton et al., 2010; Milan et al., 2011) have developed approaches to account for uncertainties when estimating volume change with combined survey techniques. In riverine environments, where significant elevation change is of the same order of magnitude as measurement uncertainty, these advances have allowed robust calculations of complete geomorphic volume change with associated uncertainty and significance testing. In the coastal environment, where study sites may be large (Okm), with significant regions of limited change (e.g. near the depth of closure), it is important to robustly deal with uncertainty as errors can rapidly propagate to misrepresent large proportions of the observed change. Until now, there has been a distinct lack of full embayment supra to sub-tidal sediment budget assessments within the coastal environment, due to the lack of coexisting spatial and temporal data sets, and the difficulty/lack of accounting for uncertainty in survey methods (Schimel et al., 2015).

In the longer term, inter-annual variability in the winter-averaged wave climate is strongly affected by atmospheric changes (Bacon and Carter, 1993; Clarke and Rendell, 2009; Dodet et al., 2010; Castelle et al., 2017a, 2017b). Strong relationships exist between phases of climatic indices and variations in wave height and storm characteristics. On a basin wide scale, Barnard et al. (2015) found that coastal erosion across 48 different Pacific Ocean beaches, was significantly linked with variations in the El Nino Southern Oscillation (ENSO), whilst Mortlock and Goodwin (2016) showed on a regional scale, that different modes of ENSO produced variations in wave power from subtly different directions, causing a discrepancy between erosion and recovery rates within an embayed headland beach in south east Australia.

In the Northern Hemisphere, the North Atlantic Oscillation (NAO), is known to affect the incoming wave climate in the northern latitudes of the Atlantic Ocean (e.g., Dodet et al., 2010), with particularly strong influence during winter months (e.g., Bromirski and Cayan, 2015), explaining multi-annual cross-shore change in exposed sandy beach morphology (nearshore bar configuration) in South West England (Masselink et al., 2014). Longshore rotation of macro-tidal, headland embayed sandy beaches has been well correlated to phase changes in the NAO over multiple timescales (Thomas et al., 2010, 2011, 2012), highlighting the possibility of the NAO's use as a predictor of coastline evolution. Castelle et al. (2017a, 2017b) presented a new climate index, the West Europe Pressure Anomaly (WEPA), based on the normalized sea level pressure difference between Ireland and the Canary Islands. Positive WEPA winters better describe increasing winter wave heights and increased southerly storm tracks, whilst exhibiting no significant correlation with NAO itself. Recent improvements in both the forecast skill of winter-averaged NAO (Dunstone et al., 2016), and understanding of its relationship with bi-directional wave climates (and hence beach rotational response), could provide significant advances in coastal management.

The overarching aim of this paper is to assess and quantify the morphological response of an entire gravel barrier embayment, to episodic and decadal bi-directional wave forcing. A unique series of directionally contrasting wave conditions in south west England are assessed to investigate the controls on rotational response mechanisms, from the sub embayment to full embayment extent. The study exploits a comprehensive morphological dataset collected within Start Bay (South Devon, UK), including multi-method full embayment sediment budgets, decadal records of inter-tidal beach profiles and new interpretations of connections between longer term wave climate and atmospheric variability, to further our understanding of response and recovery mechanisms within these timescales. A future goal is to improve coastal vulnerability assessment and management for coastal embayments that are sensitive to directional wave climates.

In Section 2, the regional setting and wave climate is provided. Section 3 presents the methodology and datasets used throughout the study, including comprehensive uncertainty analysis from multi-method survey data and the determination of a new parameter to predict beach rotation based on a directional wave power balance. Results are presented in Section 4, discussed in Section 5, and conclusions drawn in Section 6.

2. Regional setting – Study area

2.1. Embayment alignment and beach composition

Start Bay is a 12-km long embayment located on the south coast of Devon, UK (Fig. 1). Meso to macrotidal with neap and spring tidal ranges of 1.8 m and 4.3 m, respectively, the embayment comprises four sub-embayment gravel barrier beaches, named from the south to north as; Hallsands, Beesands, Slapton Sands and Blackpool Sands. Between each sub-embayment lie short headlands/rocky outcrops, extending to approximately 1–4 m below mean low water springs (MLWS), that separate each beach at high tide, trapping laterally moving sediment as it is transported alongshore. Behind the barrier at both Slapton Sands and Beesands, freshwater is held above mean sea level in two lagoons known as Slapton Ley and Widdecombe Ley (Austin, 2005). The gravel barrier at Slapton Sands rises to 5–6 m above mean sea level with a steep reflective beach face ($\tan\beta = 0.1$) composed of fine gravel (D50 = 2–10 mm), with the toe of the barrier extending to an average depth of −7.5 m Ordnance Datum Newlyn (ODN) (Kelland, 1975). The barrier position has remained relatively stable over the last 3000 years, allowing the sediment (mainly flint) to be reworked by the sea (Hails, 1975a). Within Start Bay, gravel is finer to the east due to the lateral grading of material (Chadwick et al., 2005), with coarser grains transported south west with larger, steeper easterly waves, and finer grains being well sorted and transported north east with smaller but more frequent southerly swells (Morey, 1976).

South of the bay lies Start Point, a rocky headland offering shelter from longer period southerly waves. Skerries Bank, an offshore banner bank, sits east of the main beaches in the southern half of the embayment and is −5 m (ODN) at its shoalest (Hails, 1975b). These two features modulate the wave climate in Start Bay. Refraction and dissipation of large southerly waves around Start Point allows waves to reach the southern sub-embayments of Hallsands and Beesands, however wave energy is reduced, resulting in an alongshore gradient in inshore wave conditions, with significant wave heights (H_s) increasing from the south to north along the embayment (Ruiz de Alegria-Arzaburu and Masselink, 2010).

Maximum water depth between the gravel barrier and the shallowest part of the Skerries Bank is −15 m ODN, deeper than the estimated depth of closure (−10 m ODN). This fact, combined with the distinct difference

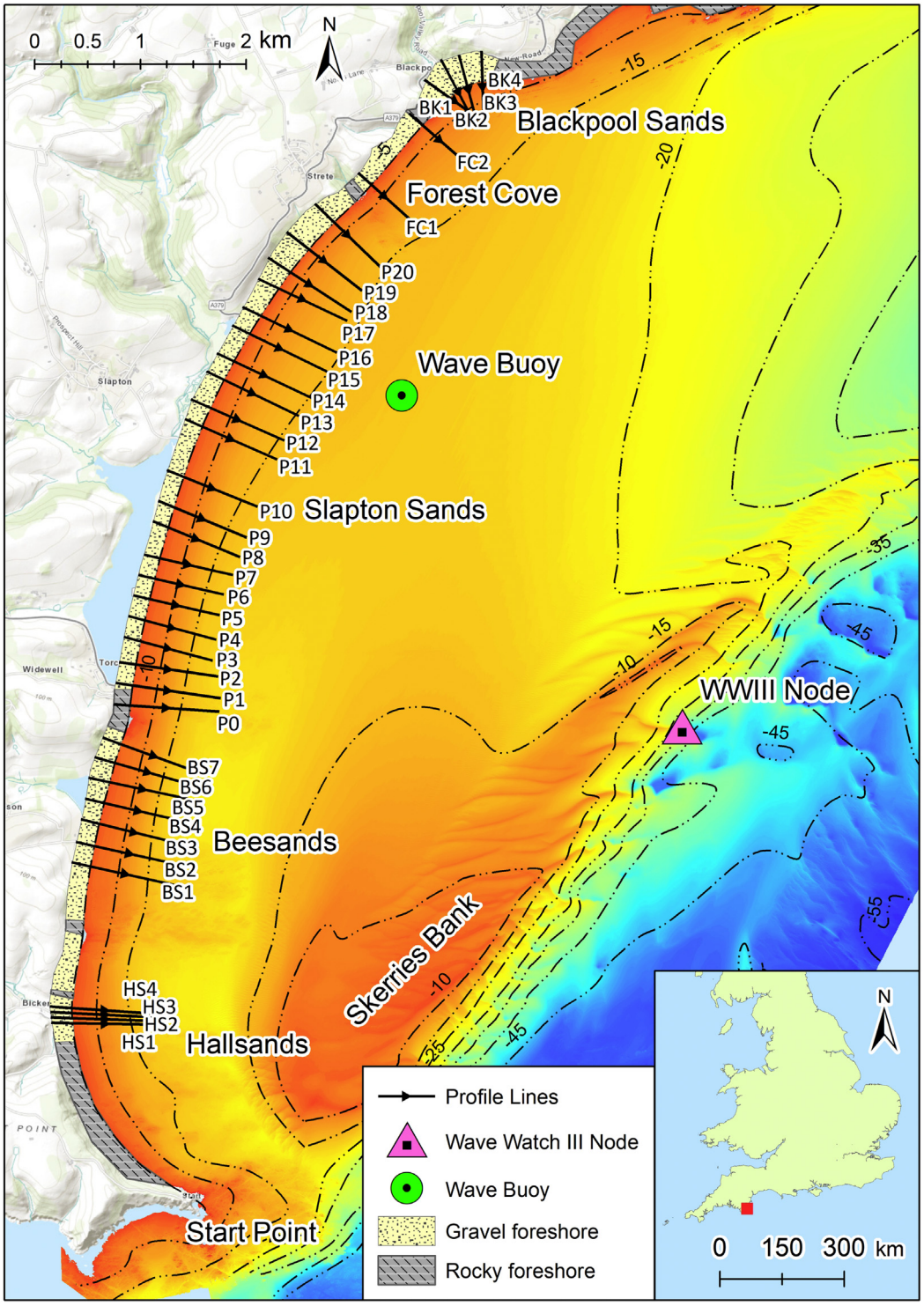

Fig. 1. Location map showing Start Bay, South Devon, UK. Nearshore bathymetry from 2013 (UKHO, http://aws2.caris.com/ukho/) and associated contours (m, ODN), highlight the location of Skerries Bank. Survey profile locations for each beach are shown as arrows pointing offshore and are labelled accordingly. The foreshore is identified as either gravel or rock, and the location of the Directional Wave Rider Buoy (http://southwest.coastalmonitoring.org/), and the WaveWatch III Model Node is shown to the east of Slapton Sands. This figure is available in colour online at https://www.journals.elsevier.com/geomorphology

in sediment type between the four gravel barriers and the finer shelly sands of Skerries Bank, suggests there is no movement of sediment between the two (Hails, 1975c). Furthermore, the entirety of Start Bay is bound by large headlands, and the system is considered a closed sediment cell, with no sediment sources except for some confined areas of cliff erosion (Ruiz de Alegria-Arzaburu and Masselink, 2010).

2.2. Wave climate – Start Bay

The local inshore wave climate has been measured since April 2007 by a Wave Rider Directional Wave buoy, located in the center of the embayment (Fig. 1) at approximately 12 m ODN water depth sampling at 30-min intervals (Plymouth Coastal Observatory, 2017). In addition to

the measured data, the UK Met Office have provided long-term 3-hourly hindcast wave data from their 8-km WaveWatch III model, between 1980 and 2017 for a node location offshore of Start Bay, in approximately 20 m water depth (Fig. 1).

The bay is aligned SSW-NNE and receives predominantly short period (mean annual T_e ~5–6 s) wind driven waves from both the south and east (Ruiz de Alegria-Arzaburu and Masselink, 2010). The long-term wave rose (Met Office hindcast) clearly shows the bi-directionality of the waves within the embayment, with a dominance of southwesterly over easterly waves (Fig. 2; bottom panel). At the model node location, south-westerly waves are propagating in the offshore direction (from the south west); however, they are refracted and attenuated towards the shoreline by interaction with Skerries Bank (Fig. 1). Previous studies (Ruiz de Alegria-Arzaburu and Masselink, 2010; Wiggins et al., 2017) have shown, through comparison with directional wave buoy records, that the dominant south-westerly waves rotate to a southerly direction at the nearshore (−12 m ODN) and easterly waves maintain their original angle. Despite nearshore transformation, the long-term offshore model hindcast record is used here for further analysis as the wave buoy data represented a relatively short time series and contained storm dropouts. Later analysis highlights the value of the longer-term offshore wave data.

The time-series of hindcast H_s (Fig. 2, top panel) shows a seasonal trend with wave heights increasing in winter (H_s = 1–1.3 m) and decreasing in summer (H_s = 0.5–0.6 m). Storm events are classified as having peak H_s exceeding 2.17 m ($H_{s5\%}$ calculated over the entire modelled wave record), with a duration of at least 6 h and separated by at least 24 h (Harley, 2017).

Since 1980, southerly waves (>110° and <240°) make up 69% of wintertime (December, January, February and March, DJFM) wave directions (Fig. 2, second panel), with a mean H_s of 1.23 m. Easterly waves (angles >60° and <110°) make up 23% of the wave directions for winter months, with average H_s of 1.15 m across the model record. High-energy southerly winter storm events are more frequent than those from the east from year to year, with a 5:1 ratio per winter; however, each year is highly variable and there are periods of dominance of storms from one direction or another.

During the winter of 2013/14, the south west of England experienced numerous, exceptionally high-energy Atlantic storms, producing the largest recorded 8-week average wave height in at least 60 years, considered the most energetic since at least 1948 (Masselink et al., 2016) with 22 storms (H_s > 5.9 m) between October 2013 and April 2014 recorded at the Seven Stones Light Vessel (50.102° N 6.100°

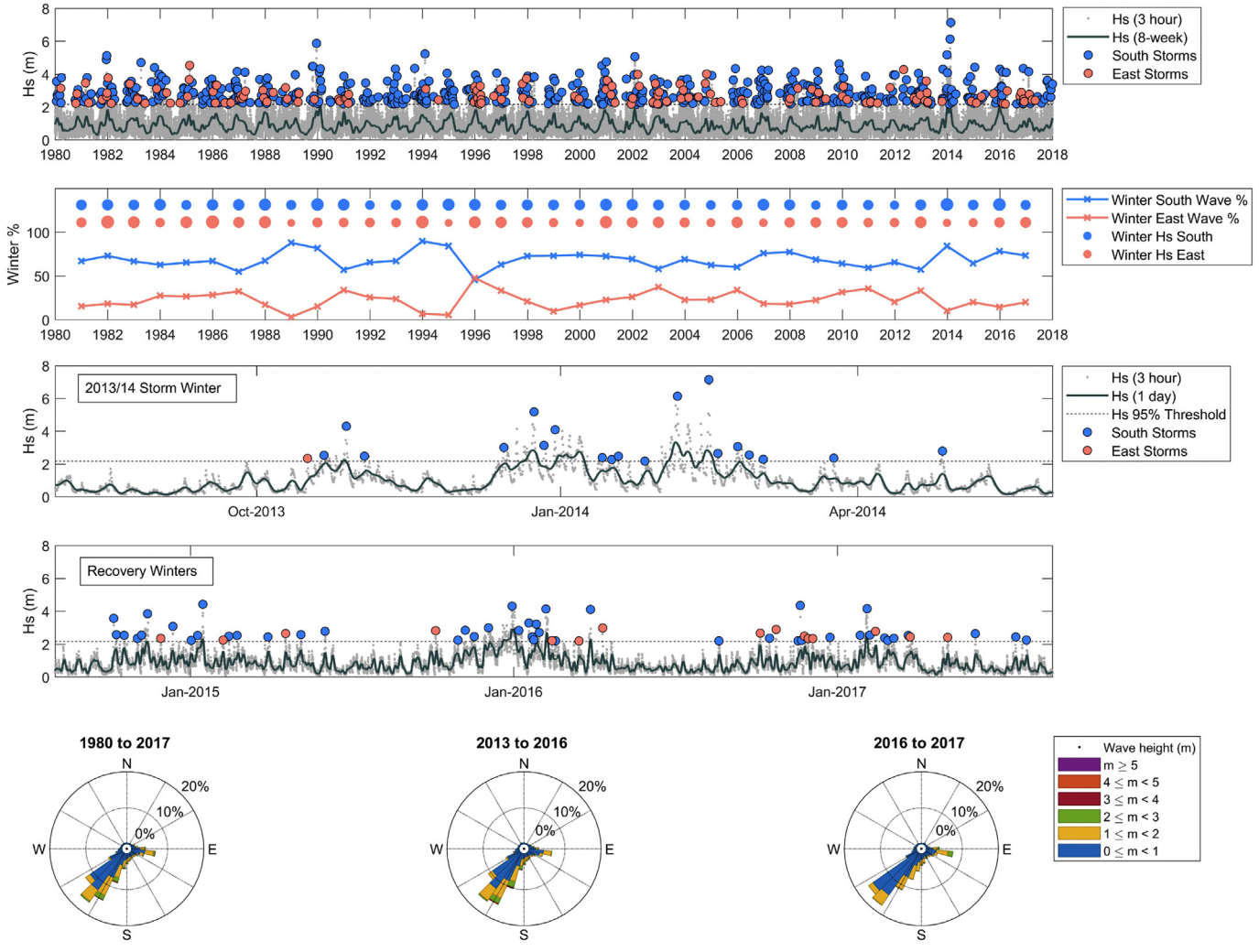

Fig. 2. Top Panel; Met Office WaveWatch III modelled hindcast data showing significant wave heights every 3 h (grey dots) and 8-week moving average (grey line) from 1980 to 2017. Associated storm events (Waves greater than $H_{s5\%}$ = 2.17 m) from both the south and east are shown by the blue and red circles respectively. Second Panel; Total winter percentages of southerly (blue) and easterly (red) wave contributions, with average wave heights for each shown by the circle size in the upper section of the panel. Third Panel; Significant wave heights of the exceptionally stormy winter of 2013/14 with a one day moving average (grey line), showing the lack of easterly storm events. Fourth Panel; Significant wave heights of the three most recent winters, with associated storm peaks highlighting the increased easterly storms of the winter of 2016/17. Bottom Panel; Wave roses from the full time series (left), 2013 to 2016 (middle) and 2016 to 2017 (right). This figure is available in colour online at https://www.journals.elsevier.com/geomorphology

W) (Masselink et al., 2015). The modelled wave data shows 15 winter storm events at the Start Bay node, characterized by a series of southerly storms with minimal input from easterlies (Fig. 2, third panel). 84% of winter waves were southerly for this period, with average winter H_s of 1.65 m, with only 10% from the east with mean wave heights of 0.70 m (Fig. 2, Second Panel). Locally, the most destructive storms within Start Bay occurred on the 04/02/2014 and the 14/02/2014 with H_s recorded at the inshore wave buoy reaching 4.69 m and 5.25 m, respectively. Compared to similar magnitude storms in this period, both incoming storms tracks from the Atlantic were south of 50° latitude and resulted in larger waves reaching the south coast of the UK. As a result, these two storms were calculated as having wave height return periods >50 years (Siggery and Wiggins, 2014) and caused the most extensive impacts on the beaches of Start Bay (Scott et al., 2016).

In the 3-year period following the winter of 2013/14, the first two winters maintained a dominance of southerly over easterly waves with the winter of 2014/15, being 65% southerly and 20% easterly in direction with average H_s of 1.14 m and 0.84 m, respectively. Further southerly waves were experienced in the winter of 2015/16, with 78% southerly waves (average H_s of 1.62 m) and only 15% easterly (average H_s of 1.12 m). A reversal in the trend occurred between 2016 and 2017, with 11 easterly storms observed between October 2016 and May 2017. Average winter values for that season show southerly waves make up 73% of wave contributions, with 20% coming from the east. Mean southerly wave heights drop to 1.06 m for that year (the lowest value for 5 years), and easterly winter waves increase to an average 1.24 m (the highest value since 2012/13).

For the purpose of the following morphological response analysis, the southerly-dominated period between 2013 and 2016, which includes the unprecedented storms of 2013/14 is considered a 'southerly' period. The significant change to easterly wave conditions from 2016 to 2017 can be considered an associated 'easterly' period, and as such, both 'southerly' and 'easterly' periods, and their effects on embayment morphology are assessed further in this study.

3. Methods and datasets

3.1. Full embayment sediment budgets

In order to calculate total sediment budgets and morphological change in a coastal embayment, it is essential to combine topographic and bathymetric survey data from different time periods. Consideration must be given to the survey instrumentation and data collection techniques, as well as the inherent uncertainty in both point cloud and gridded position and elevation (Wheaton et al., 2010). Described below are the morphological data sets used for the full embayment response analysis, as well as the approaches to gridding and addressing uncertainty.

3.2. Morphological survey data

3.2.1. Unmanned aerial vehicle (UAV) intertidal surveys

A quadcopter UAV (DJI Phantom) facilitated a full inter/supratidal survey of Start Bay in both 2016 and 2017. Implementing a structure-from-motion (*SfM*) approach (Westoby et al., 2012), overlapping aerial photographs were aligned and georeferenced using Real Time Kinematic (RTK) Global Positioning System (GPS) measured ground control points (GCP's), deriving a high-resolution (>50 pts./m^2), three-dimensional point cloud, which was then interpolated to a 1 m grid digital elevation model (DEM) of inter/supratidal beach topography. This methodology allowed full coverage of the beaches and interconnecting bays around a single set of spring tides, without significant event driven changes occurring during the data collection.

3.2.2. Multibeam bathymetry

Extending the spatial coverage of the embayment surveys into the subtidal domain, multibeam bathymetry was used from a range of sources. United Kingdom Hydrographic Office (UKHO) supplied multibeam data collected during January 2013 (UKHO, 2013), whilst Plymouth University (PU) conducted two separate surveys in June 2016 and June 2017. These data sets were surveyed at high resolutions (typically, 25 pts./m^2 point density) and exported at 1 m, providing comparable DEM's from approximately Chart Datum to below the depth of closure (≤10 m ODN).

3.2.3. Light Detection and Ranging (LiDAR)

Environment Agency UK LiDAR data is captured as part of the ongoing south west regional coastal monitoring programme (http://southwest.coastalmonitoring.org/). Datasets over Start Bay were collected during March 2012, March 2016 and April 2017. Data were supplied in a 1 m grid format, and an assessment of the measurement uncertainty has been conducted by the contractor (see Appendix).

3.2.4. Real Time Kinematic (RTK) Global Positioning System (GPS) continuous surveys

RTK-GPS continuous data was surveyed on foot at 1 Hz and covers the intertidal extent of Start Bay in areas where the UAV was unable to be utilized (due to permissions). Individual surveyors walked at 5 m spaced alongshore lines, with attention paid to capturing changes in topography and breaks in slopes (berms, crests etc.). This method was utilized for the 2013 epoch, and in some instances 2016 and 2017 to provide complete coverage of the embayment.

3.3. Full embayment Digital Elevation Models (DEM's)

The full supra/intertidal and subtidal extents of Start Bay were surveyed using the above multiple methods over three epochs, providing 'pre-southerly' (2013), 'post-southerly' (2016) and 'easterly' (2017) morphological datasets. The spatio-temporal coverage of data sets meant that multiple surveys could be combined (Fig. 3, left) producing DEMs spanning supra, inter and subtidal extents of the entire embayment to an average depth of ≤10 m ODN (Fig. 3, right).

The datasets used in this analysis and their temporal structure are summarized in Table 1. In all cases data were interpolated to a 1 m raster DEM using a natural neighbour interpolation (Sibson, 1981), which utilizes a weighted average of neighbouring points based on their respective areal contribution. It is effective in processing a high number of irregularly spaced input points, and has been shown to well represent surfaces interpolated from LiDAR point data (Bater and Coops, 2009). Whilst the 'pre-southerly' DEM comprised datasets that spanned 10 months, it was deemed appropriate in capturing the changes caused by the 2013/14 winter after assessment of a decadal, intertidal 2D morphological dataset from Start Bay, showing the significance of the event (see Section 4.3).

3.4. Quantifying full embayment geomorphic change

The basic principle of measuring geomorphic change involves the subtraction of two independent DEM surfaces to produce a DEM of Difference (DoD, Wheaton et al., 2010), with each grid cell value representing a measure of the vertical elevation difference. Individual cells can then be integrated to estimate total volume changes within the spatial extent of the DoD. A key principle when utilizing DoD's for the purpose of geomorphic change detection, is accounting for the vertical uncertainty across each DEM, and therefore an ability to discern the probability that the observed change is real (and not due to measurement or sampling error). This is particular important when attempting

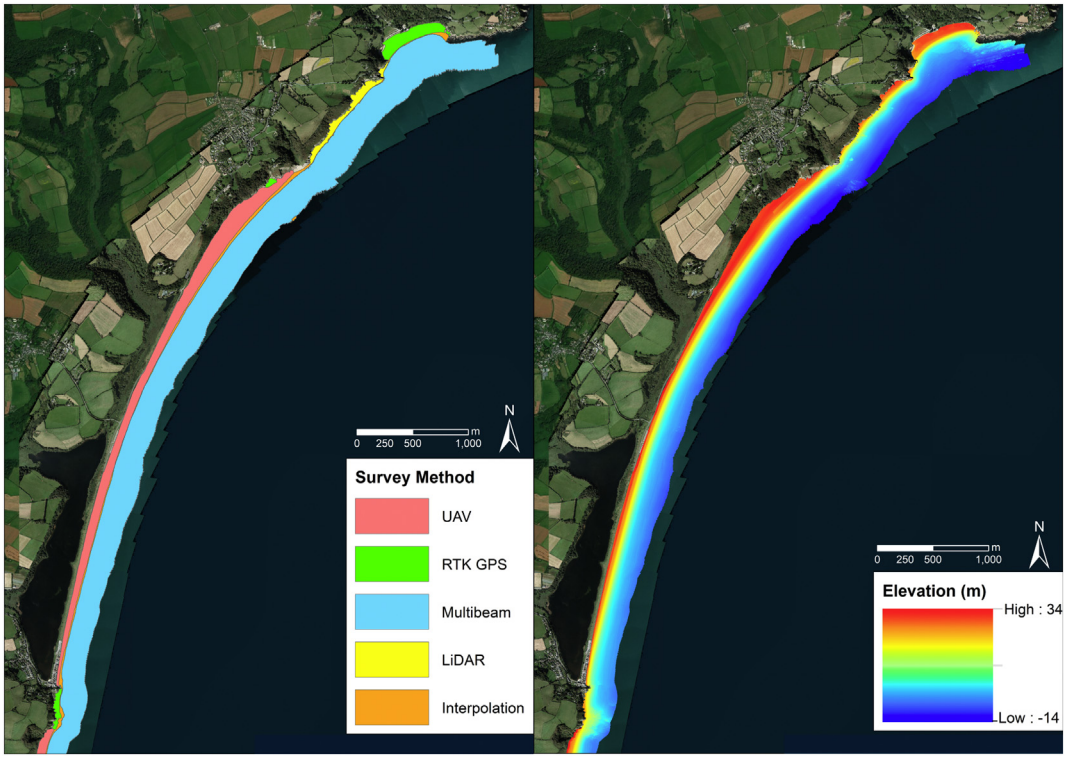

Fig. 3. Left; Example of multimethod survey masks for the northern section of the combined morphological surveys from 2016. Each colour represents the respective spatial extent covered by the individual survey techniques. Right; Example sub-section of the resultant DEM produced from a combination of survey methods. This figure is available in colour online at https://www.journals.elsevier.com/geomorphology

to detect small vertical changes (with respect to uncertainty) over broad spatial extents (Wheaton et al., 2010).

Each individual dataset has its own inherent uncertainty, based on a combination of instrument, measurement (sampling), systematic and interpolation errors. In the case of morphological surveys, variables such as the underlying surface roughness, dynamic gradients of slope, and variability in environmental conditions all contribute to the potential uncertainty of any given surface (Wheaton, 2008). Within this study (see appendix), estimates of uncertainty (δz_{DEM}) for each survey technique were obtained (Table 2) and applied to respective regions of the DEM (Fig. 3, Left).

These uncertainty estimates can then be propagated into the DoD using standard independent error propagation (Brasington et al., 2000) with the resultant propagated uncertainty (δU_{DoD}) defined as a minimum level of detection (*min*LoD);

$$minLoD = \delta U_{DoD} = \sqrt{\left(\delta z_{DEM1}\right)^2 + \left(\delta z_{DEM2}{}^2\right)} \quad (1)$$

where δz_{DEM1} and δz_{DEM2} are some metric of uncertainty from the first and second DEM respectively (Taylor, 1997). Changes measured below this *min*LoD are thresholded from the DoD and excluded from

Table 1
Temporal survey method chart highlighting the morphological survey methods used within each epoch of DEM analysis.

Morphological Survey	Year 2012	2013	2014	2015	2016	2017
UAV Intertidal (DEM 1m)					Jun	Apr
Multibeam Bathymetry (DEM 1m)		Jan			Jul	Jun
LiDAR (DEM 1m)	Mar				Mar	Apr
RTK GPS Continuous (DEM 1m)	Jul	Aug			Jun	Apr

Partial coverage
Full coverage
2013 Epoch
2016 Epoch
2017 Epoch

the total calculated change. This can be done on a cell-by-cell basis if DEM uncertainties are spatially variable.

A further conservative step can be taken when thresholding the DoD's, incorporating a probabilistic approach to assess whether the observed change is real, as set out by Lane et al. (2003). If the estimates of DEM uncertainty (δz_{DEM}) are approximated as their standard deviation of error (σ_{DEM}), and are represented by a normal distribution, a critical threshold error (U_{crit}) can be obtained using;

$$U_{crit} = t\sqrt{(\sigma_{DEM1})^2 + (\sigma_{DEM2}{}^2)} \quad (2)$$

where σ_{DEM1} and σ_{DEM2} are the standard deviations of error for the first and second DEM respectively, and t is the critical t-value for a two tailed students t-test at a chosen confidence interval (Williams, 2012). By utilizing the propagated error of the DoD on a cell by cell basis, a t score can be derived from the actual change observed such that;

$$t = \frac{|Z_{DEM_2} - Z_{DEM_1}|}{\sigma_{DoD}} \quad (3)$$

where σ_{DoD} is equal to δU_{DoD} evaluated at each cell of the DoD grid, and Z_{DEM_1} and Z_{DEM_2} are elevations from two different DEMs. The resultant t value can be related to the probability of the elevation difference occurring due to measurement error alone by utilizing the cumulative distribution function for the two tailed t test. Assuming a large number of samples is used to estimate σ_{DoD}, the t distribution is nearly identical to the normal distribution (Wheaton, 2008), such that if $t \geq 1$, the change is significant at the 68% confidence interval (1 σ).

3.5. Decadal morphology and wave climate assessment

A decadal record of quasi-quarterly RTK-GPS topographic cross-shore profiles have been collected regularly throughout Start Bay since 2007, as part of an ongoing coastal monitoring program (http://southwest.coastalmonitoring.org/). Hallsands, Beesands and Slapton Sands are surveyed three times per year on average (Spring, Summer and Autumn), whilst Blackpool Sands is surveyed twice a year (Spring and Autumn). Profile locations are shown on the map in Fig. 1, with an average line spacing of 50 m at Hallsands and 200 m at Beesands, Slapton Sands and Blackpool Sands. Measurements are made from the back beach to mean low water springs (−2 m ODN), with a maximum distance of 5 m between successive points, and additional points are taken to capture all breaks in slope to accurately represent the beach morphology. Unit volume differences relative to the first survey were then calculated for each profile.

To explore direct relationships between directionally bi-modal wave forcing and morphological change, the wave energy flux equations were used to compute the total wave power, P for the WaveWatch III modelled time series for the location of the model node (Fig. 1), using;

$$P = \frac{1}{16}\rho g H_s^2 C_g \quad (4)$$

where ρ = water density, g = gravity, H_s = the significant wave height and C_g = the wave celerity based on the wave energy period T_e and local water depth h, using linear wave theory for intermediate depths.

Wave power was then split into southerly (240°> and >115°), and easterly (<60° and <115°) directions, and an index of the normalized balance of the two contributions was obtained by Eq. (5);

$$D : P_{index} = \frac{(P_{south} - P_{east}) - \overline{(P_{south} - P_{east})}}{\sigma(P_{south} - P_{east})} \quad (5)$$

where $(P_{south} - P_{east})$ is the difference between the southerly and easterly wave power, $\overline{(P_{south} - P_{east})}$ is the long-term average of those winter differences, and $\sigma(P_{south} - P_{east})$ is the long-term standard deviation of winter differences, calculated over the entire model record from 1980 to 2017.

This index, hereinafter referred to as the directional power index ($D : P_{index}$), was calculated for each time interval between successive morphological surveys at each profile. Positive and negative values for $D : P_{index}$ represent the dominance of southerly and easterly waves respectively, in comparison to the long-term mean. The index was then plotted against the measured volume changes between morphological surveys, and linear correlation coefficients were obtained for the relationship between the two. This correlation was further split from total correlations (using the entire record), into winter correlations (using only volume changes and wave power indexes observed during winter months (December to March).

3.6. Climatic indices and winter wave variability

The influence of climate indices on waves in the North Atlantic is stronger in the winter months due to the increased occurrence of storm events; hence, in this study, a normalized winter-averaged (DJFM) value of the station-based NAO index is utilized (Hurrell et al., 2017). Further to the NAO, winter-averaged values of WEPA (Castelle et al., 2017a, 2017b) are presented as an additional climate index, and both are assessed against with the long-term winter modelled wave record.

4. Results

4.1. Multi-annual southerly and easterly full embayment response

Computed significant morphological change across the southerly period (2013–2016) indicated strong northward transport of sediment within the embayment as a whole, and within individual sub-embayments, manifesting in a pronounced clockwise rotational response (Fig. 4, left). Significant sub-aerial erosion was recorded at the southern end of sub-embayment beaches, whilst accretion was observed at the northern ends with material collecting at rocky headlands.

The net change across the whole embayment is highlighted in Fig. 5 (top) and shows the balance of erosion and accretion. Overall, a total thresholded volume of 641,900 m^3 of erosion was observed, with a thresholded deposition of 593,300 m^3. A net volume thresholded change of −48,600 m^3 was observed, which falls within the propagated uncertainty of the analysis (±91,300 m^3) and is therefore not significant at the 95% confidence limit. As a result, the system has to be observed as closed, with no significant detectable net loss or gain of sediment through either barrier over wash, offshore transport or longshore flux beyond the extreme southern or northern extents of the embayment.

During the easterly phase (2016–2017) the geomorphic change analysis highlights a reversal in the rotational response of Start Bay (Fig. 4, right). Erosion is observed at the northern ends of all sub-embayments, with an associated accretion observed at the southern ends. The strongest areas of erosion occurred at the northern end of Slapton Sands and Forest Cove. The thresholded DoD analysis (Fig. 5, bottom) shows the full embayment experienced a total erosion of 289,700 m^3 whilst gaining 241,500 m^3. The net change equates to −48,200 m^3, which, like the 2013 to 2016 analysis, is within the associated uncertainty of the analysis (±61,900 m^3), suggesting that there has again been no detectable net loss or gain of material within the embayment. A distinct pivot point for the full embayment is observed across both epochs at the northern end of Slapton Sands, around the location of P18 (Fig. 1), where erosion and accretion are clearly delineated. The total volume changes past this point were calculated for both epochs, with 529,500 m^3 (±54,500 m^3) transported north of this point between 2013 and 2016, and only 139,218 m^3 (±24,630 m^3) passing southward of this point between 2016 and 2017.

Table 2
Summary of survey method, uncertainty type, calculated value and the source of analysis.

Survey type	Uniform or variable	Calculated uncertainty (σ)	Source of analysis
RTK - GPS topographic continuous	Uniform	0.054 m	Reference surface comparison
UAV structure from motion	Uniform	0.038 m	Reference surface comparison
Airborne LiDAR (2012/2017)	Uniform	0.150 m	GPS ground truth
Multibeam bathymetry 2013	Fixed	0.270 m	IHO Order 1a specification
Multibeam bathymetry 2016	Variable	0.08–1.830 m	Spatially variable CUBE surface
Multibeam bathymetry 2017	Variable	0.03–0.158 m	Spatially variable CUBE surface

Comparisons of the two epochs show that total detectable volume change measured from 2016 to 2017 is 45% of 2013 to 2016, however; this anti-clockwise rotation occurred within a single annual cycle, spanning a winter period containing a higher percentage of easterly waves than the previous two (Fig. 2, Bottom Right), highlighting the importance of wave direction in controlling beach morphology.

4.2. Sub-embayment morphological response

Dividing the full embayment into individual sub-embayments (Fig. 4, green boundaries), definitive erosional and accretional responses are observed across the measured time periods. Sub-embayments were defined as beach sections between clear protrusions of rock headlands, or where clear interfaces were observed in the rotational response. The spatial redistribution of sediment is shown though volume change histograms for each sub-embayment (Fig. 6), including the associated uncertainty from the DoD calculations.

Large volumes of sediment were lost and gained during the southerly dominated 2013–2016 epoch (Fig. 6 Left column), with significant and detectable net losses in all four southern sub-embayments (Hallsands, Hallsands South, Beesands and Slapton Sands). Net volume gains were observed at the northern sub-embayments of Forest Cove and Blackpool Sands. The resultant imbalance of erosion and accretion within individual sub-embayments, but insignificant net full embayment change, suggests there is either cross-shore exchange of sediment, or an alongshore flux of material bypassing headlands and transitioning between sub-cells.

To assess the cross-shore element of sediment transport within sub-embayments, profiles were extracted across the full-embayment surveys at 50 m intervals, and the relative contributions of sub-aerial (≥2 m ODN) and sub-tidal (≤2 m ODN) volume change was calculated (Fig. 7).

During the 2013–2016 epoch (Fig. 7, upper), substantial in-phase change occurred in both the sub-aerial and sub-tidal elevations, particularly at the northern extents of Beesands, Slapton Sands and Blackpool Sands. Within Beesands, profile BS1 at the southern extent lost 91 m^3/m, with 32% occurring in the sub-tidal extent. The northernmost profile, BS7, gained 178 m^3/m with sub-tidal changes making up 47% of the total volume accreted. Similar results are observed at Slapton Sands, with P1 losing 126 m^3/m in the south (20% sub-tidal losses) and P20 gaining 524 m^3/m (33% sub-tidal accretion) in the north. Throughout the embayment, the sub-tidal sediment volume changes are in phase with sub-aerial changes and the detectable depth of closure has been reached (Fig. 7). These results, in combination with the balanced total sediment budget for both epochs suggest that there is no significant cross-shore exchange causing the net volume disparity within sub-embayments, and that the only mechanism for the large-scale changes is bypassing of material around headlands from one embayment to the next. The integrated volume change in the sub-tidal extent is approximately 33% of the total volume changes observed across all profiles within the full embayment, illustrating the significant contribution sub-tidal change makes to the total sediment budget.

During the 2016–2017 easterly epoch, sub-embayment anti-clockwise beach rotation was observed at Beesands, Slapton Sands and Blackpool Sands (Fig. 4, Right), although no significant net gains or losses were detected (Fig. 6 Right). This suggests that there has been no detectable flux of sediment into or out of the three major sub-embayments. The only significant sub-embayment net volume change (in comparison with that lost during the southerly epoch) was within the north of the embayment. Forest Cove experienced a net loss of −56,000 m^3, compared to a gain of +89,000 m^3 between 2013 and 2016. As Forest Cove represent a transition cell between Blackpool Sands and Slapton, this loss is explained as a detectable southward flux of sediment out of the sub-embayment into Slapton Sands.

The measured geomorphic changes during the southerly and easterly epochs show that the entire embayment rotated in a clockwise direction under the extreme southerly-dominated conditions of 2013 to 2016, with headland bypassing evidenced as large-scale redistribution of material between sub-embayments. Under the easterly conditions of 2016 to 2017, anti-clockwise rotation was observed within sub-embayments, with absolute change approximately 40% of the southerly epoch; however, minimal net changes occurred through headland bypassing, indicating volume changes induced across the entire embayment in 2013–2016 have not returned.

4.3. Decadal morphological change and forcing mechanisms

Whilst spatially integrated total embayment response provides invaluable understanding of response and recovery mechanisms to extreme variability in the wave climate, an extended temporal record is required to quantify the relationship between wave forcing and morphology.

The changes to the beach profile volumes across the embayment over the last ten years (Fig. 8) show there is an underlying trend of accretion at profiles in the northern embayment of Blackpool Sands (BK1 and BK2 gaining 31 and 38 m^3/m per year respectively), and the northern end of Slapton Sands, with P19 accreting at 23 m^3/m per year. The central and southern section of Slapton Sands has shown a negative trend in volume difference since 2007, with P9 and P2 losing at respective rates of −8 and −12 m^3/m per year. The trend is similar at Beesands, with volume losses in the south (BS2 eroding at −10 m^3/m per year) matched by gains in the north (BS7 accreting at 3 m^3/m per year). Profile volumes at Hallsands have shown a semi-stable response, with positive and negative changes occurring from 2007 until the stormy winter of 2013/14, after which the beach volume has significantly decreased, remaining depleted in the years since.

The significance of the 2013/14 southerly storm response is clear from the volume change plots, as the largest profile volume changes occurred over this period. The effect of this winter on the long-term profile volume trends is significant, in many cases doubling the rates of erosion or accretion calculated between 2007 and summer 2013. Profiles in the northern sections of sub-embayments, which accreted during the storms, have generally remained stable, and in some cases, continued to increase in volume since 2014. Conversely, southerly profiles have continued to erode and only shown signs of accretion in the last year from 2016 to 2017. The 2013/14 winter is the only event in the time series that experienced significant full embayment rotation with headland bypassing.

Correlations between $D : P_{index}$ and short-term (~3-monthly) morphological change over a decade of observations show that the balance of southerly to easterly wave power directly controls the spatial variation of beach volumes, with correlations stronger in the winter when absolute wave energy is greater (Fig. 9).

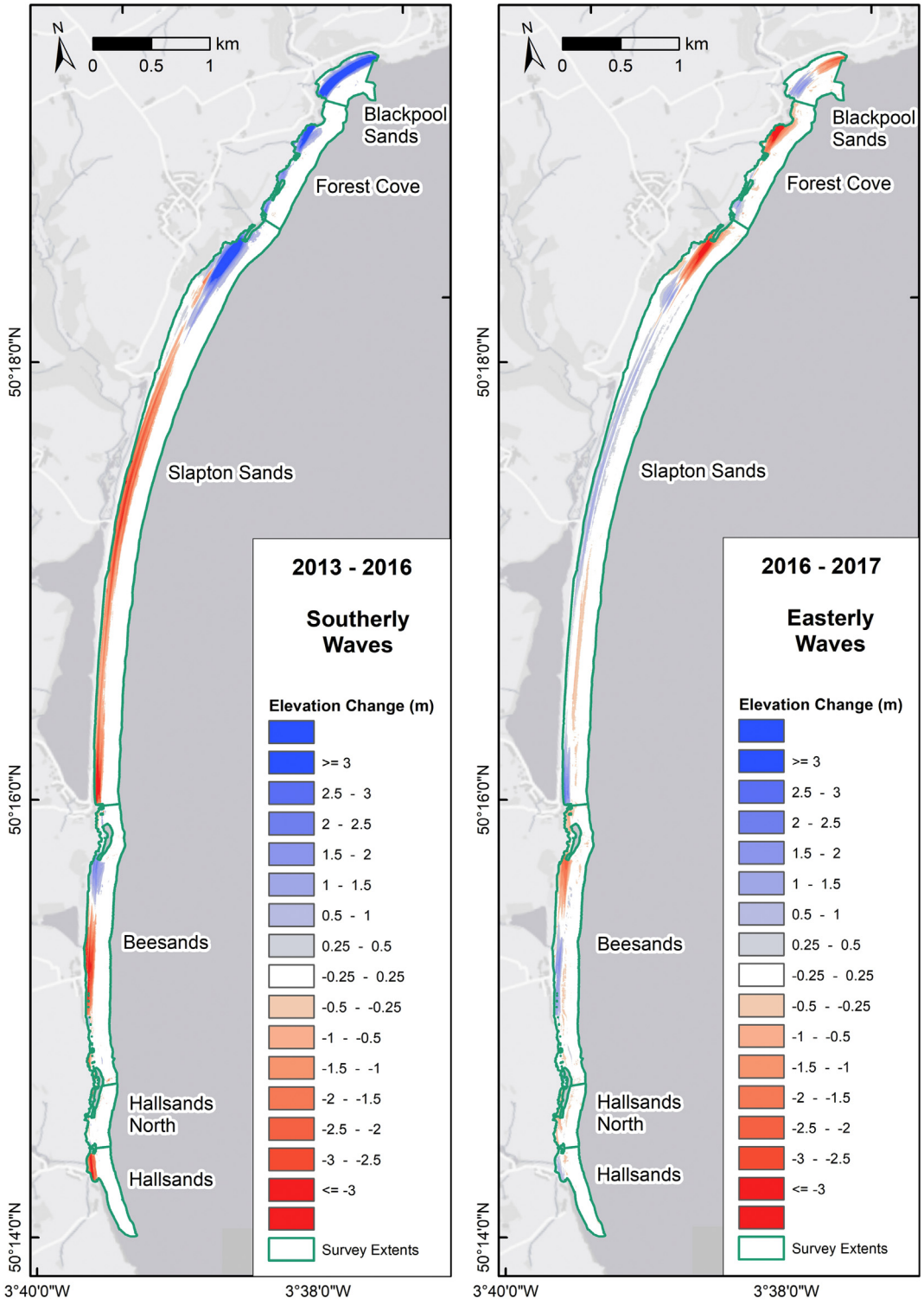

Fig. 4. Thresholded DoD's for the southerly period between 2013 and 2016 (Left) and easterly period between 2016 and 2017 (Right). Elevation changes between epochs are represented as colour intensity from red (erosion) to blue (accretion), with no detectable change represented as a lack of colour. This figure is available in colour online at https://www.journals.elsevier.com/geomorphology

Profiles at the southern (northern) extents of sub-embayments show the strongest negative (positive) correlations. Where the correlation is strongly positive (>0.7), such as at the northern extents of Beesands, Slapton and Blackpool Sands, profiles gain volume under southerly dominated wave conditions, and lose volume under predominantly easterly wave conditions. The converse is true, for example at Hallsands and the southern extents of Beesands and Slapton Sands, where negative correlations (≤0.7) indicate a loss of sediment under southerly waves, and a gain of material under easterly dominated conditions. Two distinct rotational pivot points are evidenced by the alongshore correlations at both Beesands and Slapton Sands (Fig. 9). Between profile BS5 and BS6, correlations switch from negative to positive, meaning under southerly

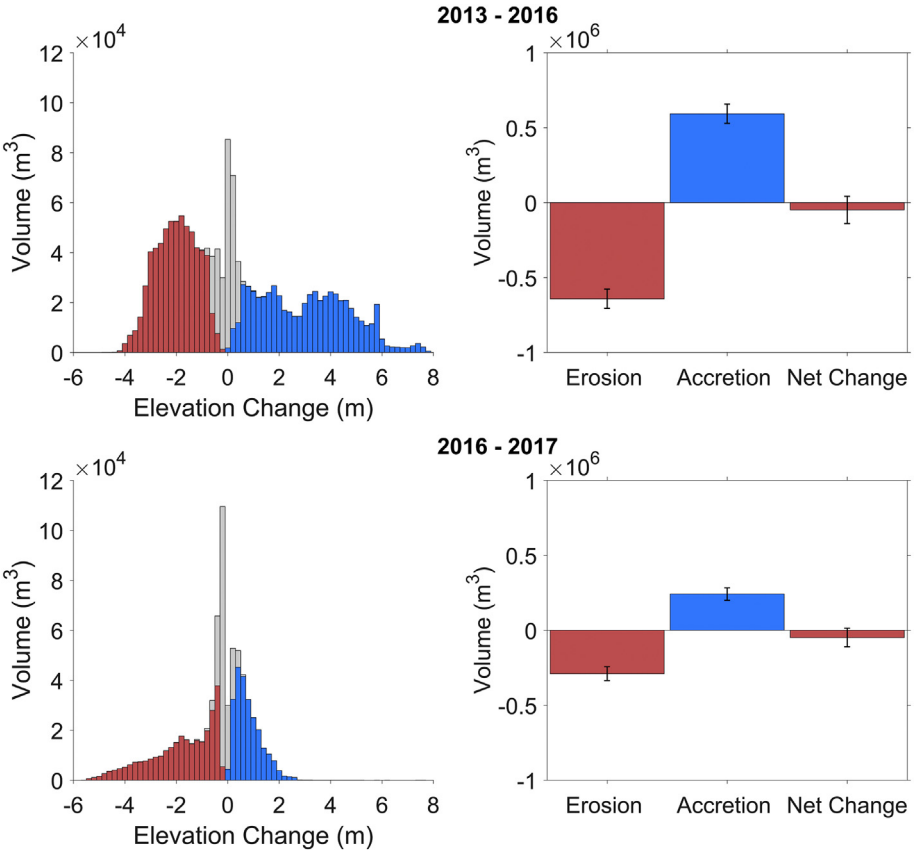

Fig. 5. Thresholded volume change within Start Bay between during the southerly period of 2013 and 2016 (top panel), and easterly period between 2016 and 2017 (bottom panel). Volume elevations changes are expressed in terms of erosion (red) and accretion (blue) (Left Panels). Grey bars represent volume change in which elevation differences were below the LoD, and hence were thresholded from the total volume calculation. Total and net volume changes within the embayment (Right Panels), expressed in terms of erosion (red) and accretion (blue). The black error bars represent the propagated volume uncertainty at the 95% confidence interval associated with the result. This figure is available in colour online at https://www.journals.elsevier.com/geomorphology

dominated wave conditions, the Beesands sub-embayment erodes to the south of this point and accretes to the north. A similar pivot point is observed at the northern end of Slapton Sands, with correlations again switching from negative to positive around profile P18. The full embayment difference models (Fig. 4) also evidence these two pivot points, with clear transitions from erosion and accretion found in similar locations under both southerly and easterly wave conditions.

Strong correlations (both positive and negative) between the $D : P_{index}$ and beach volume change at sub-embayment extremities, shows that the offshore modelled waves are well correlated to measured beach morphology, despite not being transformed inshore, suggesting that directionality of incoming wave power is a key component in predicting beach change.

4.4. Role of atmospheric variability

The wave climate presented in Fig. 2 shows that the winter-averaged contribution from each directional mode varies dramatically on a multi-annual to decadal timescale. From the morphological response in the short-term, it is clear that this has a significant impact of the direction and magnitude of embayment rotation. The next intuitive step is to examine the link between climate indices and dominant wind and wave directions to investigate their explanatory power for multi-annual winter-average bi-directional balance and hence long-term morphological response.

The long-term winter modelled wave data since 1980 shows the dominance of southerly over easterly wave power (Fig. 10; Upper); however, the offshore waves cannot be compared in absolute terms, due to the lack of inshore transformation. The most energetic winters within the model record were 1990 and 2014 and are attributable almost exclusively to southerly wave events. Easterly wave power contributes <40% of the total winter wave power with the exceptions of 1986 and 1995 (Fig. 10, Lower). The $D : P_{index}$ for the entire modelled record is shown in Fig. 10 (Middle), and highlights where the balance of winter wave power is either more southerly dominated than average (positive) or more easterly dominated than average (negative). Multi-annual periodicity linked to variations in incident wave direction are evidenced by sustained periods of positive or negative winter $D : P_{index}$ values, for example the five year positive period between 1998 and 2002 and the following four year negative phase between 2003 and 2006 (Fig. 10, Middle). This leads to an assessment of whether fluctuations in atmospheric climate indices can account for or predict changes in the direction of the incoming wave climate and therefore the rotational beach morphology observed at this location.

Winter-averaged values of the NAO and WEPA index from 1980 to 2017 are plotted against the winter-averaged wave parameters and presented in Fig. 11. The $D : P_{index}$ exhibits only a moderate positive correlation with winter NAO values ($R = 0.48$; $p = 0.0043$), however; there is a significant negative correlation between winter NAO and easterly deep-water wave power ($R = -0.73$; $p = 0.0000$). Further examination shows southerly winter wave power is weakly correlated with winter NAO ($R = 0.28$; $p = 0.1116$). Therefore, it can be assumed the low correlation with southerly waves is reducing the relationship with $D : P_{index}$. This could be explained by the southerly wave power dependence on storm track latitude which is ill-defined by the NAO as elaborated by Castelle et al.

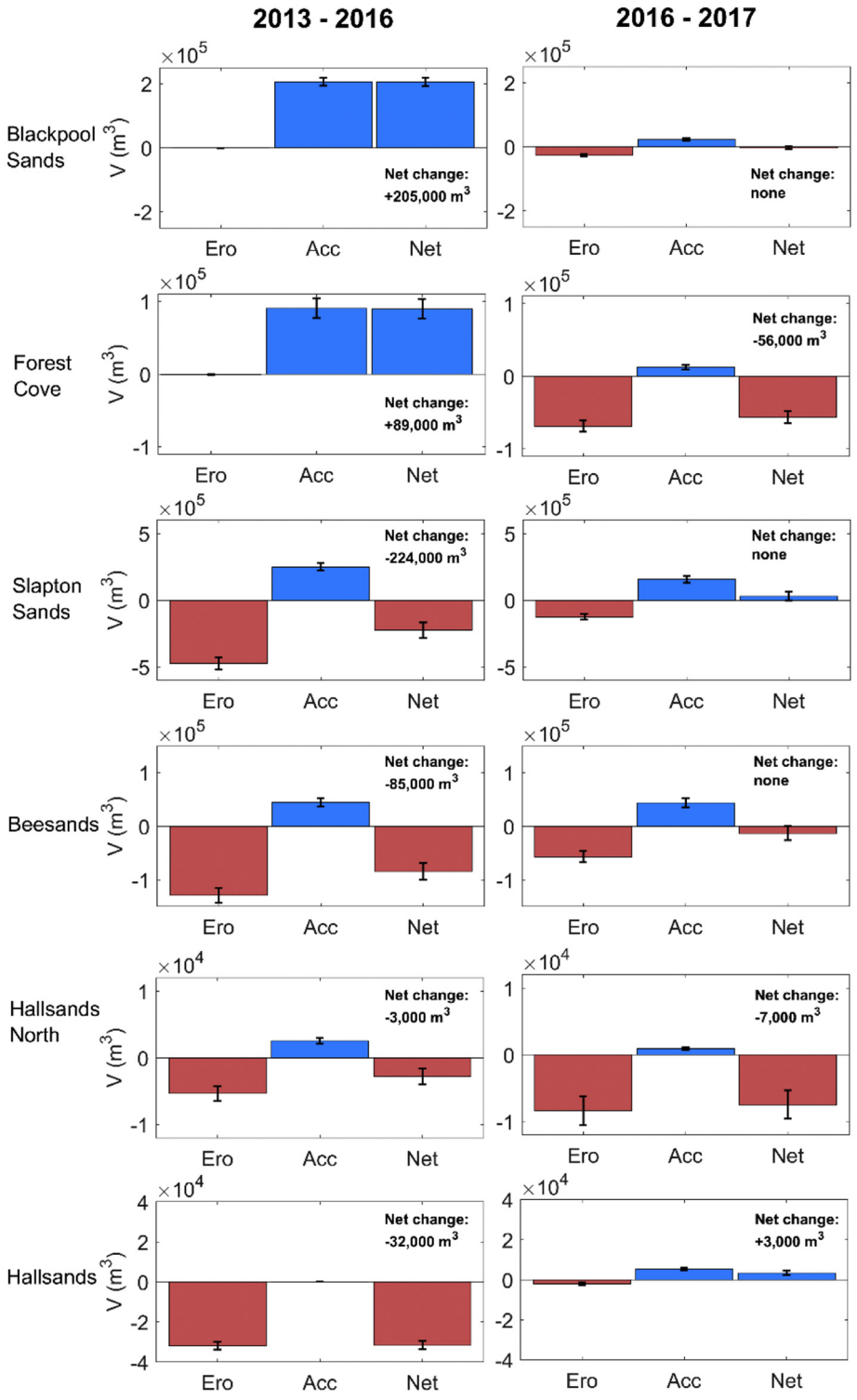

Fig. 6. Total volumetric change within sub-embayments from 2013 to 2016 (Left) and 2016 to 2017 (Right) - note the differing Y axis limits between sub-embayments. Black bars represent the uncertainty estimates for the total combined erosion, accretion and net change. Net detectable change is displayed on each plot. Where change was less than the total propagated uncertainty, no net change is quoted. This figure is available in colour online at https://www.journals.elsevier.com/geomorphology

(2017a, 2017b), therefore the NAO may provide skill in describing the balance of easterly and southwesterly wave events through the presence or lack of easterly wave events at this location.

The WEPA index, developed by Castelle et al. (2017a, 2017b) for explaining lower latitude wave climate (western Europe), provides an improved relationship with bi-directional waves, especially those from the southwest (Fig. 11, bottom panels). A significant positive correlation between winter WEPA and both the D : P_{index} ($R = 0.69$; $p = 0.0000$) and southerly winter wave power ($R = 0.81$; $p = 0.0000$) is observed. There is no significant correlation between winter WEPA and easterly winter wave power (Fig. 11, Lower-middle).

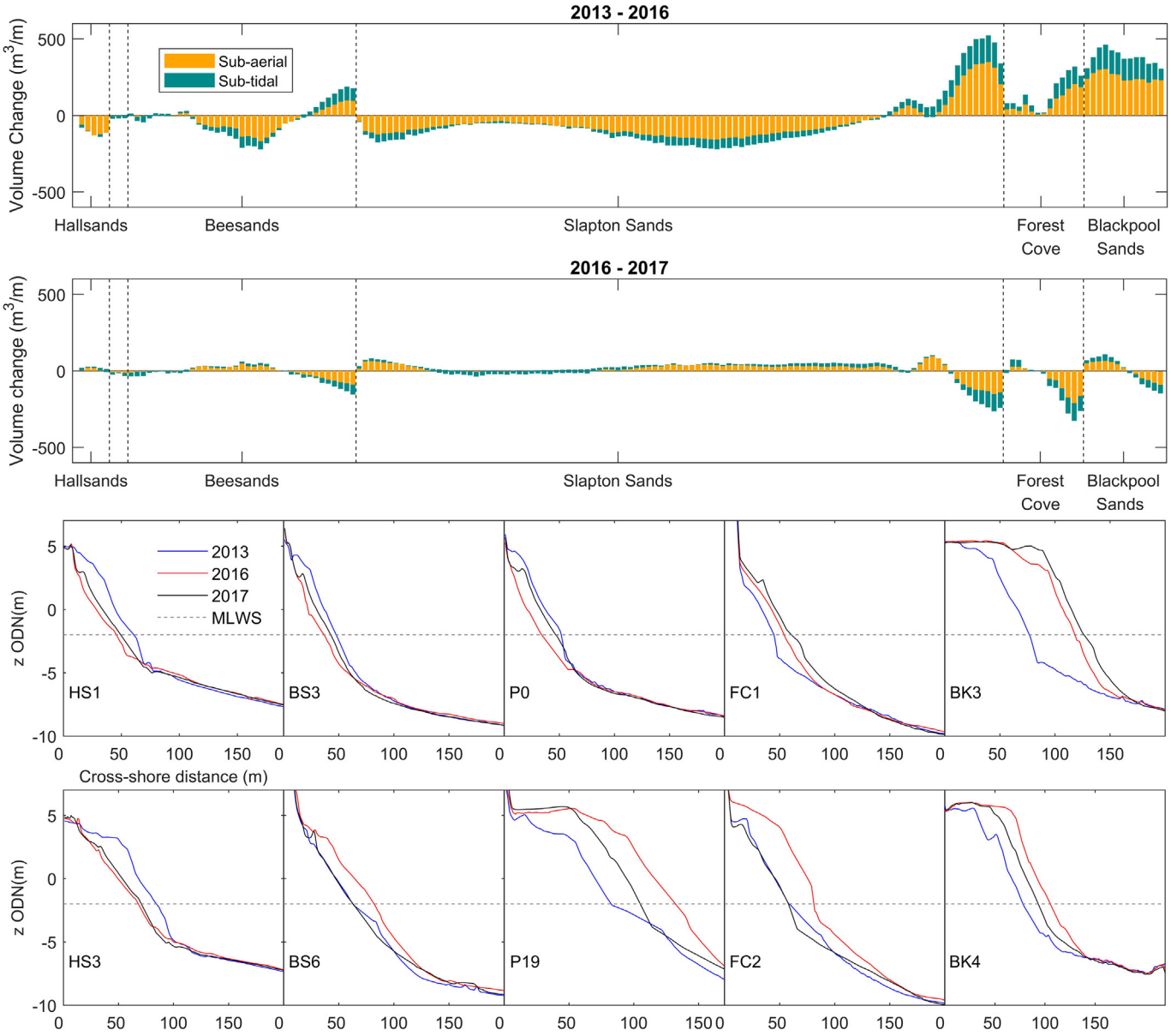

Fig. 7. First and second panel. Extracted profile volume change from 2013 to 2016, and 2016 to 2017, showing intertidal and sub-tidal (≤2 m ODN) contributions. Vertical dashed lines represent the relative location of headlands between sub-embayments. Profile elevations are presented in the lower panels. This figure is available in colour online at https://www.journals.elsevier.com/geomorphology

5. Discussion

5.1. Full embayment extreme winter response

Beaches dominated by a rotational response to wave forcing occur worldwide, particularly semi exposed coastlines with bi-directional wave climates, where headlands or structural constraints trap sediment transported alongshore at embayment extremities. This study has quantified and examined the full morphological response of a semi-sheltered gravel embayment to a multi-annual bi-directional wave climate, including a >1:50 year winter storm season. Similar to previous studies of rotational beaches, the findings here highlight that beach rotation is a function of wave direction over a variety of timescales. At event and winter-averaged seasonal scale (e.g. Ruiz de Alegria-Arzaburu and Masselink, 2010; Thomas et al., 2011), energetic storms prevailing from one direction have the ability to cause significant and rapid changes to the planform shape and sediment distribution within rotational embayments. Klein et al. (2002) suggested that seasonal rotation often results in erosion and accretion at opposite ends of an embayment, but does not lead to net sediment losses; however, under the exceptionally southerly-dominated storm conditions during the winter of 2013/14, initial assessments of a single sub-embayment (Slapton Sands, Scott et al., 2016) highlighted the net loss of sediment from the inter-tidal extent. These losses were accounted for in this study, by the calculation of total sediment budgets including all sub-embayment beaches within the full embayment, at both sub-aerial and sub-tidal extents. Through well-defined and thoroughly assessed uncertainty bounds (following Wheaton et al., 2010) significant changes were identified to have occurred between sub-embayments with a new level of confidence, accounting for more of the total sediment budget, across all sediment pathways (e.g. Goodwin et al., 2013), improving the understanding of spatial patterns of embayment response to storms. The occurrence of full embayment rotation between 2013 and 2016, with 33% of significant geomorphic changes occurring in the sub-tidal extent (up to 47% in some locations); represents a considerable proportion of the sediment

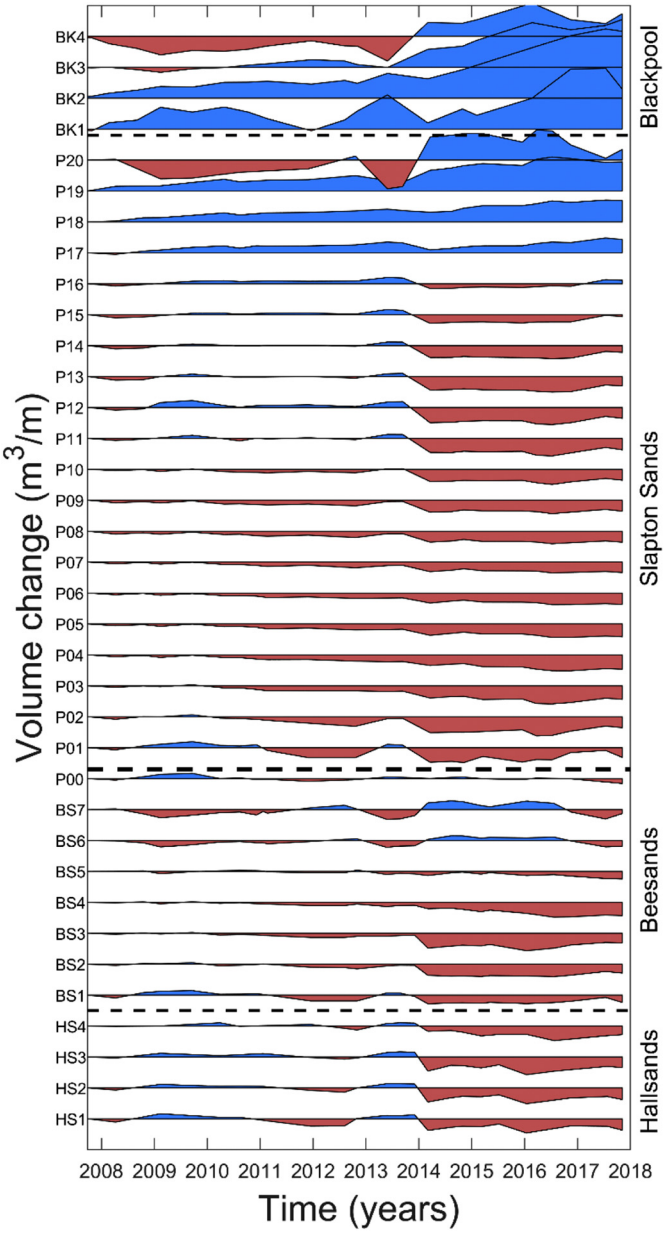

Fig. 8. Volume change time series for intra annual profiles in Start Bay, collected between 2007 and late 2017 by PCO. Profiles are displayed from north to south (top to bottom), with Blackpool Sands at the top of the figure, and Hallsands at the bottom. The red dashed line indicates the separation of sub-embayments by headlands. Volume change at each profile is shown relative to the first survey in 2007 and represents volume change as a unit of beach width (m^3/m). This figure is available in colour online at https://www.journals.elsevier.com/geomorphology

budget that would have been unaccounted for using conventional inter-tidal or sub-aerial measurements alone. Furthermore, net sediment losses and gains from individual sub-embayments highlight sediment bypassing headlands, being transported from one sub-embayment to the next, as suggested by Burvingt et al. (2018).

5.2. Sub-embayment counter rotation to easterly waves

The anti-clockwise (southward) sub-embayment rotation observed between 2016 and 2017 following the increased but moderate easterly wave conditions (20% contribution of winter easterly waves compared to the long-term mean of 23%) of that winter resulted in volume changes that were ~50% less than those observed between 2013 and 2016. As a consequence, sub-embayments counter-rotated, but sediment exchange between headlands was minimal. Scott et al. (2016) hypothesized that a rebalance of an embayment towards its pre-storm state would require aggregated equal and opposite wave events from the east. The changes observed in this study suggest that for sub-embayments to restore pre-storm sediment volumes, specific wave conditions must prevail that drive not only reversals in sediment transport direction but occur at absolute magnitudes and timescales that allow sediment to traverse back around headlands already bypassed, resulting in full embayment rotation. These conditions were not met during the 2016–2017 epoch of this study, and headlands acted to constrain sediment changes to sub-embayment rotation only.

Many geological, geometrical and hydrodynamic factors affect the facilitation of transport around headlands, including the bathymetric slope angle, headland apex ratio, protrusion length or size, as well as the occurrence of a shore platform (George, 2016). The headlands within Start Bay are complex and varied and hydrodynamics and geological orientation will play equally important roles. Headland bypassing within embayed coastlines may be asymmetrical, with some headlands "open" to transport under one set of wave conditions, but "closed" under another. This has significant implications for the understanding of recovery of sediment losses, suggesting full embayment rotation is dependent on the occurrence of headland bypassing, requiring a specific cumulative threshold of absolute wave power from one direction, rather than simply a reversal of wave angle. If such conditions are not met, recovery of sediment may be impossible without human intervention, and coastal vulnerability at up-drift locations may be permanently increased. Future work underway will look to improve our understanding of the mechanisms governing gravel (bedload transport) bypassing of headlands and conditions required to allow sediments to transition from one sub-embayment to the next.

5.3. Decadal embayment response to wave climate variability

Over longer timescales, this study developed and utilized the $D : P_{index}$, a new equilibrium parameter, used here to describe the imbalance of opposing southerly and easterly wave power relative to the long-term mean. For the interim period between morphological profile surveys over a decadal scale, strong correlations (both positive and negative) were observed between the $D : P_{index}$ and beach volume change at sub-embayment extremities. These results suggest that the direction of longshore transport and its control on beach morphology is linked with not just the occurrence of high-energy episodic wave events, but also the dynamic balance of incident wave power from southerly and easterly directions. Observed correlations with beach morphology are strongest for changes measured during the winter months (Fig. 9), due to high energy wave events in the North Atlantic occurring most frequently between December to March (van Nieuwkoop et al., 2013; Wolf and Woolf, 2010), where the seasonal clustering of storm events is greatly affected by atmospheric oscillations (Castelle et al., 2017a). Peak period (spectral energy) from the WWIII hindcast data was used for wave power calculations. This approach does not resolve the spectral contributions of wind and swell (bi-directional or otherwise). This is deemed acceptable as the focus is on alongshore transport (rotation) rather than cross shore profile shape. Previous studies have shown that gravel barrier shape responds differently to spectral contributions of swell and wind waves (e.g. Mason et al., 2009; Bradbury et al., 2011).

Whilst morphological response here is well correlated with incident wave direction, the long-term winter wave climate shows significant multi-annual variability for both the total wave power, and the southerly and easterly contributions to the bi-directional wave balance (Fig. 10). Previous studies have identified links between atmospheric climate variability and incident wave heights, with particular focus on the North Atlantic Oscillation (Bacon and Carter,

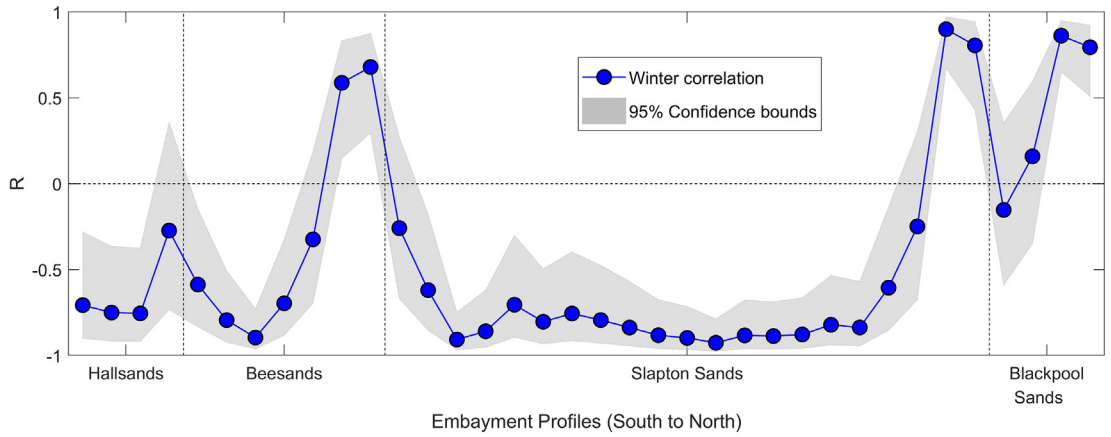

Fig. 9. Winter correlation coefficients (with associated 95% confidence intervals) between observed intertidal volume change and $D : P_{index}$ for the decadal time series of inter-tidal beach profiles within Start Bay. This figure is available in colour online at https://www.journals.elsevier.com/geomorphology

1993; Masselink et al., 2014) and the El Nino Southern Oscillation (Barnard et al., 2015; Barnard et al., 2017; Mortlock and Goodwin, 2016) for the Atlantic and Pacific Oceans respectively. Castelle et al. (2017b) identified that the NAO index did not capture the unprecedented stormy winter of 2013/14, characterized by increased southerly storm tracks (Masselink et al., 2015) and full embayment rotation at Start Bay, and devised the WEPA index to better characterize increased wave heights in more southern latitudes of the European North Atlantic coast. Santos et al. (2017) explored the link between the magnitude and frequency of extreme wave heights

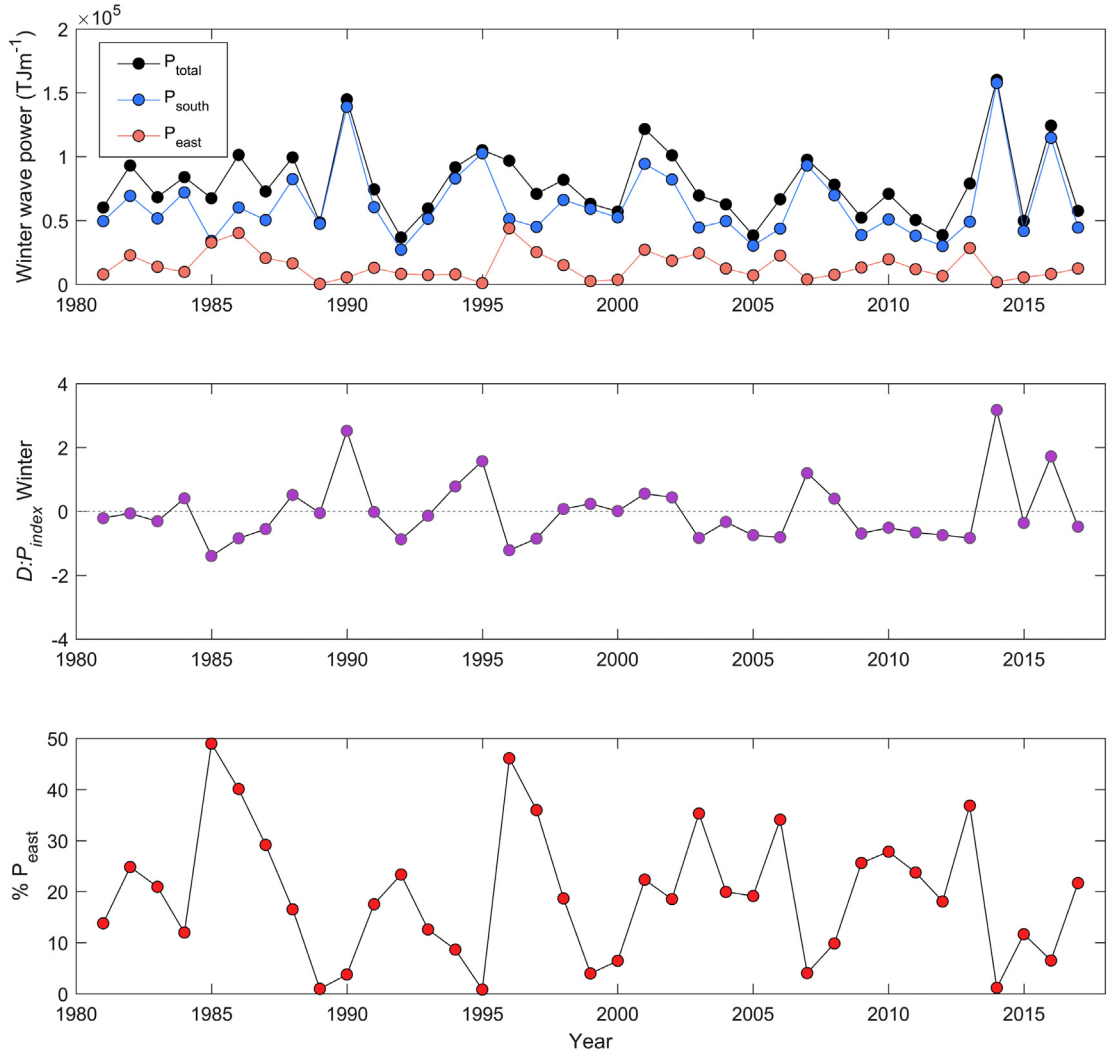

Fig. 10. Upper; winter (DJFM) wave power total (black), westerly (blue) and easterly (red). Middle; Southerly to Easterly wave power index ($D : P_{index}$) computed for the winters of the modelled wave record. Lower; easterly wave power as a percentage of the total wave power for each winter. This figure is available in colour online at https://www.journals.elsevier.com/geomorphology

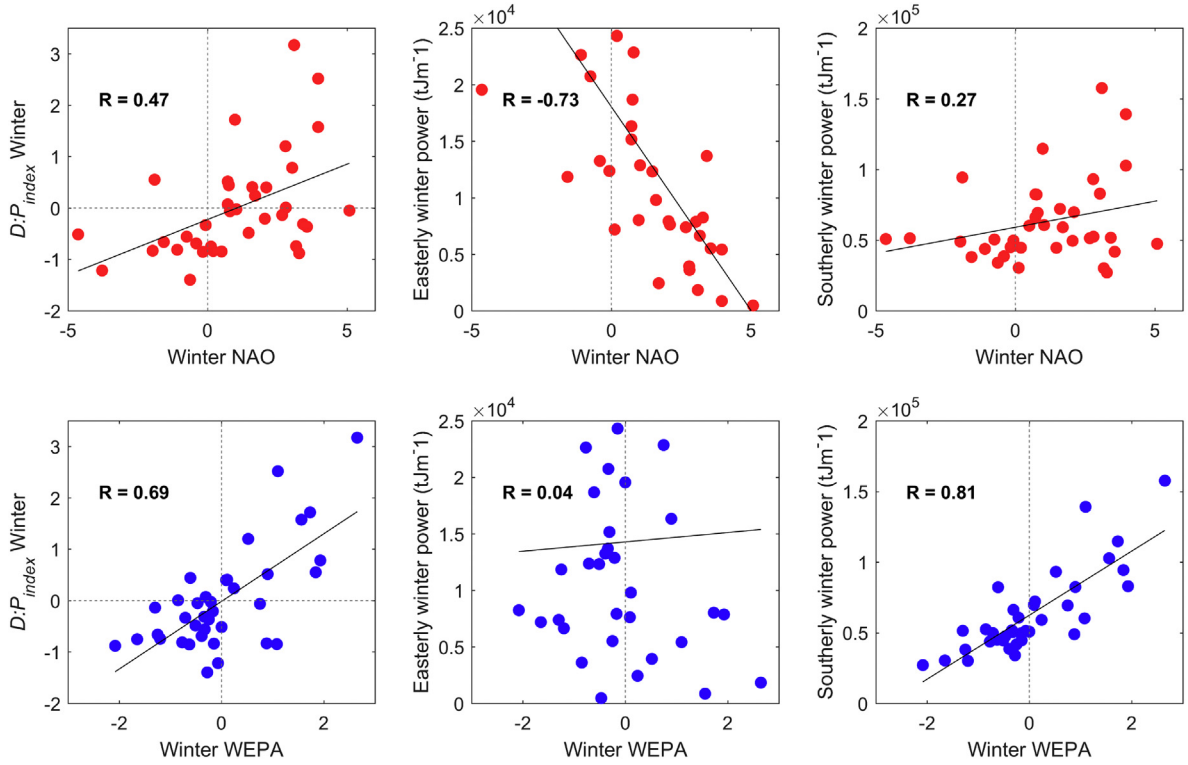

Fig. 11. Upper; Winter NAO versus winter wave parameters: $D : P_{index}$ (upper-left panel), easterly wave power (upper-middle panel), southerly wave power (upper-right panel). Lower; Winter WEPA versus wave parameters: $D : P_{index}$ (lower-left panel), easterly wave power (lower-middle panel), southerly wave power (lower-right panel). This figure is available in colour online at https://www.journals.elsevier.com/geomorphology

around the UK and concluded that WEPA is better suited to predicting wave action in the south west than the NAO; however, their dataset was temporally limited to 10 years of wave buoy data per site, and direction of wave events was not considered. In this study, it is shown for the first time, that the two dominant winter wave directions, easterly and southerly, are significantly correlated with winter-averaged NAO ($R = -0.73$) and WEPA ($R = 0.81$), respectively.

Long-term wave climate controls over the 37-year record are summarized in Fig. 12, with the four winter variables (NAO, WEPA, $D : P_{index}$ and relative wave power) showing two distinct modes, representing northward (clockwise) and southward (anti-clockwise) rotation. The top-right quadrant (Fig. 12) indicates winters with positive NAO (suppressing easterlies), and positive WEPA (increased southerly storm tracks). These winters are typically dominated by large southerly storms (large red circles, Fig. 12-left) and are associated with the strongest northward transport. The bottom-left quadrant represents periods of negative NAO (allowing Easterlies to develop), and negative WEPA (fewer southerly storm tracks), associated with a relative dominance of easterly conditions ($D : P_{index}$ is uniformly negative), and dominant southward transport within Start Bay. The top-left and bottom-right quadrants of Fig. 12 indicate periods where the relevant climate indices are in opposition, and net rotation direction is uncertain. These findings are consistent with the correlation found between cross-shore volume transport and the WEPA index, on the northern exposed coastline of the south west UK (Burvingt et al., 2018). This suggests that climate indices are useful predictors of morphologic change on a wide range of exposed, to semi-exposed coastlines.

These findings indicate that, respectively, winter-averaged NAO and WEPA are effective in explaining the easterly and southerly wave components driving morphological change in Start Bay. Therefore pressure-driven climate scale indices can account for the observed bi-directional periodicity in wave climate in this study. It is therefore expected that atmospheric indices like the NAO, may skillfully explain long-term wave climate variability in other (semi) sheltered environments significantly influenced by bi-directional waves. Further work will explore the use of WEPA and NAO to forecast seasonal changes to wave climate and beach morphology. Recent modeling breakthroughs in seasonal forecasting of the winter NAO (Dunstone et al., 2016) suggest there may be an applicable level of skill in 3-month forecasting of winter NAO (Stockdale et al., 2015). The recent growth in ensemble size is increasing the skill of such models, allowing predictions of winter NAO to take place up to one year in advance (Dunstone et al., 2016; Wang et al., 2017; Scaife et al., 2015). If these models can be validated and improved, allowing the combined prediction of NAO and WEPA (Castelle et al., 2018), governments and coastal engineers may be able to plan using event and seasonal scale forecast wave conditions, acting before potential changes in beach morphology result in increased coastal vulnerability.

6. Conclusions

This study examines extreme event and decadal sub and full-embayment rotation within a headland embayed gravel coastline with a bi-directional wave climate. We highlight the importance of antecedent morphology and storm sequencing in transitioning from sub-embayment to full embayment rotation. Over multi-annual timescales, morphological change is correlated with the wave power balance from the two dominant directions, which in turn are correlated with atmospheric indices.

Under the dominance of a particular wave direction, individual sub-embayments may rotate; however, if persistent seasonal or extreme energy levels exceed a given threshold, significant headland bypassing can occur, leading to full-embayment rotation.

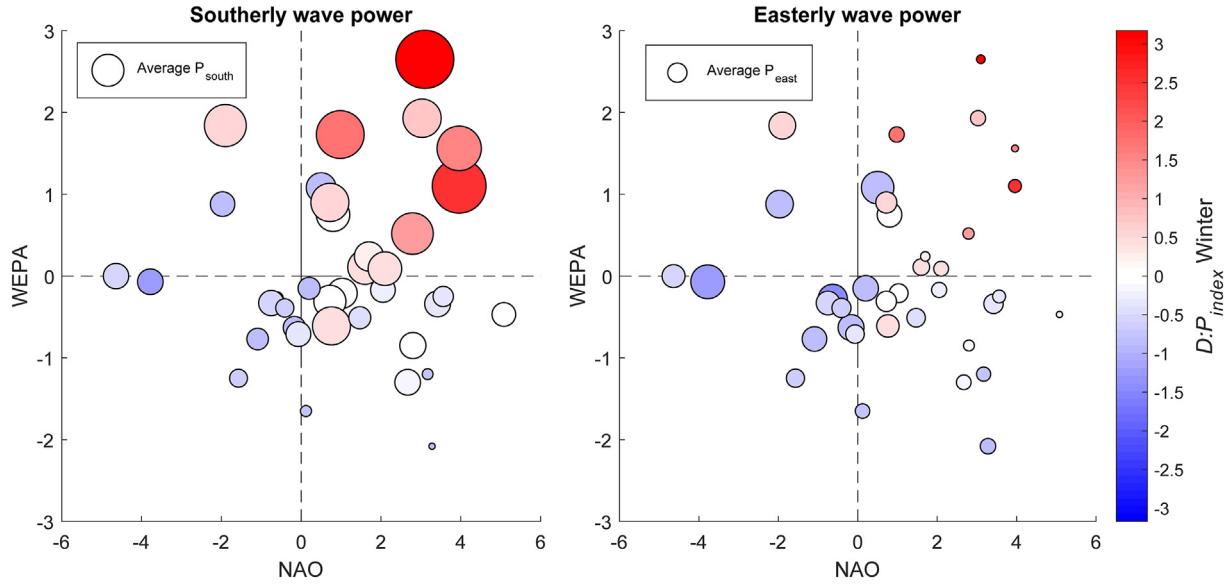

Fig. 12. Summary plot of winter values for NAO vs WEPA, with $D : P_{index}$ values represented by circle colour, and winter contributions of relative wave power from southerly (Left) and easterly (Right) waves represented by circle size. This figure is available in colour online at https://www.journals.elsevier.com/geomorphology

1. During a >1:50 year energetic southerly winter (2013/14), extreme wave events from one direction resulted in full embayment rotation; whereas, persistent moderate energy from the alternate easterly wave direction (2016–2017) resulted in sub-embayment rotation, failing to reach the threshold required for headland bypassing and full embayment rotation.
2. A total sediment budget approach, including all sub-embayments and sub-tidal extents (with robust spatial uncertainty assessments), are required to fully understand the geomorphic response mechanisms in rotational embayments.
3. Beach rotation can be parameterized by a new index that quantifies the deviation in the directional wave balance between the two dominant directions from the long-term average.
4. Winter wave direction is correlated with two distinct climate indices, suggesting that atmospheric oscillations may explain periodicity and multiannual morphological changes at embayed rotational sites with bi-directional wave climates.

Findings presented here help advance our understanding of event-scale, annual, and decadal embayment morphological response mechanisms. This new knowledge should help improve coastal vulnerability assessment and management in embayments sensitive to directional wave climates.

Acknowledgments

This work was supported and partly funded by the UK Natural Environment Research Council (NE/M004996/1; BLUE-coast project). Additional data was provided by the Plymouth Coastal Observatory, United Kingdom Hydrographic Office, containing public sector information licensed under the Open Government Licence v3.0., United Kingdom Meteorological Office, The Climate Data Guide and Bruno Castelle. The authors would like to acknowledge QPS and Trimble for support in the collection of data and processing software. Thanks also go to all beach surveyors in the collection of data, particularly Peter Ganderton, Aaron Barrett, Nieves Garcia Valiente, Olivier Burvingt and Oliver Billson.

Appendix A. Uncertainty assessments

For each survey method and subsequent DEM, an estimate of the uncertainty is required. Various approaches can be taken, ranging from simple instrument accuracy values quoted by manufacturers, to full investigations into the error budget of a single survey (Lichti et al., 2005). In this study, independent analysis was conducted to obtain reasonable uncertainty values that can be applied to each DEM. In each case, the uncertainty estimate represents the total combined integration of all individual sources of error including instrument, measurement, systematic and interpolation, and is therefore site-specific.

A.1. Subaerial uncertainty

To quantify uncertainty estimates for both the UAV and RTK-GPS continuous data, a reference surface was produced for comparison with each survey method. A typical stretch of the embayment was surveyed using a Leica terrestrial laser scanner (TLS), with reference targets measured with a total station. This allows the total combination of all sources of uncertainty to be incorporated, using the same sampling methods employed during data collection. The resultant laser scan was used as a reference point cloud (>100 pts./m^2), with vertical errors below one centimeter (RMSE = 0.005 m). A UAV survey was conducted simultaneously, using ground control points surveyed using RTK GPS (RMSE <0.030 m). A surveyor conducted a continuous topographic survey on the same stretch of beach, walking with an RTK-GPS rover measuring position and elevation data at 1 Hz. The reference surveys were interpolated to a 1-m grid, using the same technique as applied to final multimethod DEM's. Each respective raster was subtracted from the laser scan surface providing a direct measure of uncertainty, results are summarized and presented in Fig. A1 and Table A1.
In all cases, third-party processed LiDAR point data passed ground truth comparisons with RTK-GPS data points on immovable objects, and results quote a vertical accuracy within 1σ of 0.150 m. LiDAR data has been used from 2012 and 2016 where there are no other sources of topographic data. In other instances, where notable change has occurred, for example at the back of the active beach, LiDAR has been used in combination with other data sources to extend the spatial extent of individual DEMs.

A.2. Sub-tidal uncertainty

An alternate methodology was needed to address the uncertainty within the multibeam surveys, as it was not possible to obtain an absolute sub-tidal reference control surface. A combined statistical and

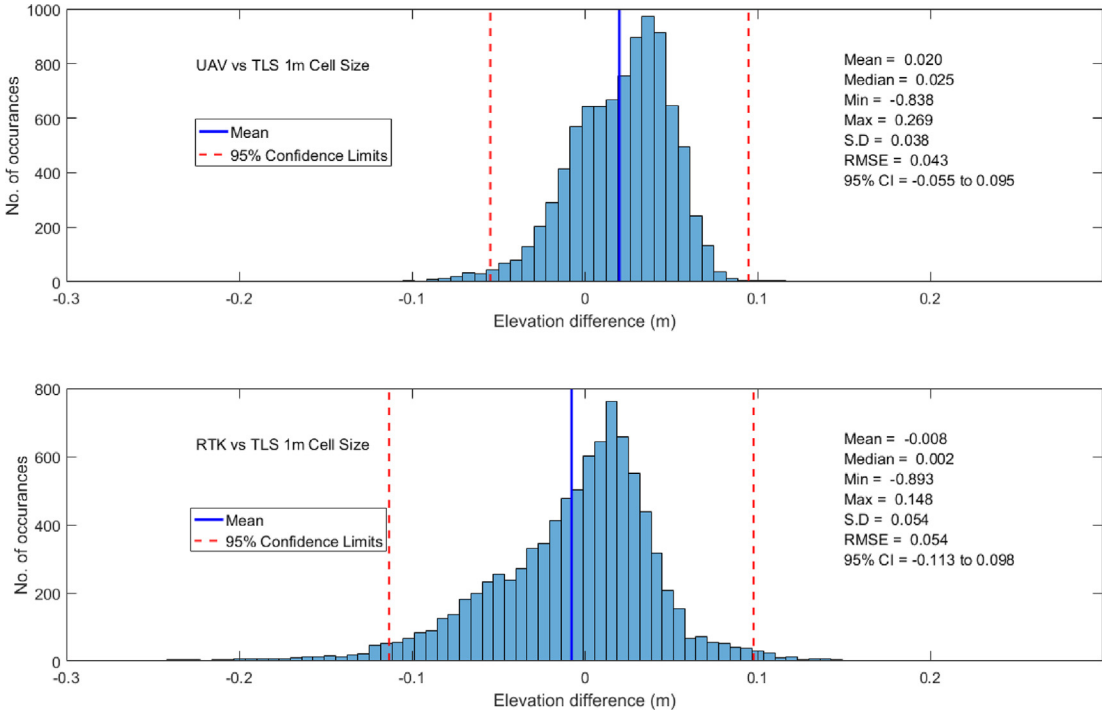

Fig. A1. Upper; histogram of elevation differences between 1 m DEM created from TLS reference survey, and DEM from UAV survey. Lower; Histogram of elevation differences between 1 m DEM created from TLS reference survey, and 1 m DEM from RTK GPS walking survey. This figure is available in colour online at https://www.journals.elsevier.com/geomorphology.

Table A1
Comparison of UAV and RTK GPS surveys against a laser scan reference survey. Statistics are presented for the raster to raster comparison.

Comparison with laser scan reference	Raster to raster 1 m cell Z differences (m)							
	Mean		Median		S.D		RMSE	
	Vector	Absolute	Vector	Absolute	Vector	Absolute	Vector	Absolute
UAV	0.020	0.031	0.025	0.029	0.038	0.030	0.043	0.043
RTK GPS	−0.008	0.037	−0.002	0.027	0.054	0.040	0.054	0.054

error budget modeling approach was taken based on a priori estimates of uncertainty of system components, computed in QPS QINSy/Qimera survey acquisition software, to generate total propagated uncertainty (TPU) values for each individual sounding. These were then gridded across the multibeam survey region using the Combined Uncertainty and Bathymetric Estimator (CUBE) algorithm, which provides a statistically robust method for generating spatially variable residual uncertainty surfaces (Calder and Mayer, 2003; Calder and Wells, 2007; Schimel et al., 2015). The range of uncertainty values for the 2016 and 2017 data are given in Table A2, with the highest values occurring over high roughness regions (rock reefs) and at swathe edges, and lowest values over flatter sandy regions directly beneath the sonar. As no TPU values were available for the 2013 survey (secondary dataset) a conservative estimate based on the known survey specification (International Hydrographic Organization Order 1a; IHO, 2008) was used, providing a spatially uniform uncertainty value (1 standard deviation from the mean (σ) quoted as $\pm$0.270 m).

To address the lack of an absolute control surface to assess influence of systematic error between the surveys, a reference surface analysis was conducted across a flat immobile rocky seabed region 50 m × 50 m and at −14 m ODN depth. The roughness length scale of the selected region was an order of magnitude less than the width of the control region to minimize incorporation of significant vertical errors due to any horizontal misalignment. To minimize random error orthogonal lines were run and only data from beam angles between $\pm$45° were used to compute the mean elevation differences from 0.5-m gridded surfaces for each survey. Due to lack of immobile reference region options, no other areas could be compared so it is unknown if these error values are variable across the domain. Therefore, based on this analysis and using 2017 survey as a reference (utilized GNSS Post Processed Kinematic heighting), appropriate fixed vertical offsets (representing systematic errors) were applied during volume change calculations.

Table A2
Elevation difference statistic for Multibeam reference region (0.5-m gridded).

Survey	Start bay 2017–2016	Start bay 2017–2013
Area	50 m × 50 m (−14 m ODN)	50 m × 50 m (−14 m ODN)
S.D	0.07 m	0.08 m
Mean	−0.05 m	−0.20 m
Median	−0.06 m	−0.19 m
RMSE	0.07 m	0.22 m

References

Austin, M.J., 2005. Swash, Groundwater and Sediment Transport Processes on a Gravel Beach. Ph.D. Thesis. Department of Geography, Loughborough University, UK.

Bacon, S., Carter, D.J.T., 1993. A connection between mean wave height and atmospheric pressure gradient in the North Atlantic. Int. J. Climatol. 13, 423–436. https://doi.org/10.1002/joc.3370130406.

Barnard, P.L., Short, A.D., Harley, M.D., Splinter, K.D., Vitousek, S., Turner, I.L., Allan, J., Banno, M., Bryan, K.R., Doria, A., Hansen, J.E., Kato, S., Kuriyama, Y., Randall-Goodwin, E., Ruggiero, P., Walker, I.J., Heathfield, D.K., 2015. Coastal vulnerability across the Pacific dominated by El Niño/Southern Oscillation. Nat. Geosci. 8, 801.

Barnard, P.L., Hoover, D., Hubbard, D.M., Snyder, A., Ludka, B.C., Allan, J., Kaminsky, G.M., Ruggiero, P., Gallien, T.W., Gabel, L., McCandless, D., Weiner, H.M., Cohn, N., Anderson, D.L., Serafin, K.A., 2017. Extreme oceanographic forcing and coastal response due to the 2015-2016 El Niño. Nat. Commun. 8, 1–8. https://doi.org/10.1038/ncomms14365.

Bater, C.W., Coops, N.C., 2009. Evaluating error associated with lidar-derived DEM interpolation. Comput. Geosci. 35, 289–300. https://doi.org/10.1016/j.cageo.2008.09.001.

Bergillos, R.J., Ortega-Sánchez, M., Masselink, G., Losada, M.A., 2016a. Morpho-sedimentary dynamics of a micro-tidal mixed sand and gravel beach, Playa Granada, southern Spain. Mar. Geol. 379, 28–38.

Bergillos, R.J., López-Ruiz, A., Ortega-Sánchez, M., Masselink, G., Losada, M.A., 2016b. Implications of delta retreat on wave propagation and longshore sediment transport-Guadalfeo case study (southern Spain). Mar. Geol. 382, 1–16.

Bergillos, R.J., Masselink, G., Ortega-Sánchez, M., 2017. Coupling cross-shore and longshore sediment transport to model storm response along a mixed sand-gravel coast under varying wave directions. Coast. Eng. 129, 93–104.

Bradbury, A., Stratton, M., Mason, T., 2011. Impacts of wave climate with bi-modal wave period on the profile response of gravel beaches. Proceedings of Coastal Sediments. World Scientific 3, pp. 2004–2018.

Brasington, J., Rumsby, B.T., McVey, R.A., 2000. Monitoring and modelling morphological change in a braided gravel-bed river using high resolution GPS-based survey. Earth Surf. Process. Landf. 25, 973–990. https://doi.org/10.1002/1096-9837(200008)25:9<973::AID-ESP111>3.0.CO;2-Y.

Bromirski, P.D., Cayan, D.R., 2015. Wave power variability and trends across the North Atlantic influenced by decadal climate patterns. J. Geophys. Res. Ocean. 120, 3419–3443. https://doi.org/10.1002/2014JC010472.

Burvingt, O., Masselink, G., Russell, P., Scott, T., 2016. Beach response to consecutive extreme storms using LiDAR along the SW coast of England. J. Coast. Res., 1052–1056 https://doi.org/10.2112/SI75-211.1.

Burvingt, O., Masselink, G., Russell, P., Scott, T., 2017. Classification of beach response to extreme storms. Geomorphology 295, 722–737. https://doi.org/10.1016/j.geomorph.2017.07.022.

Burvingt, O., Masselink, G., Scott, T., Davidson, M., Russell, P., 2018. Climate forcing of regionally-coherent extreme storm impact and recovery on embayed beaches. Mar. Geol. 401, 112–128. https://doi.org/10.1016/j.margeo.2018.04.004.

Calder, B.R., Mayer, L.A., 2003. Automatic processing of high-rate, high-density multibeam echosounder data. Geochem. Geophys. Geosyst. 4 (1048). https://doi.org/10.1029/2002GC000486.

Calder, B.R., Wells, D., 2007. CUBE User's Manual – Version 1.14. University of New Hampshire, USA.

Castelle, B., Dodet, G., Masselink, G., Scott, T., 2017a. The West Europe Pressure Anomaly (WEPA): a simple sea-level-pressure based climate index controlling winter wave heights along the western coast of Europe from Portugal to UK (36–52°N). Proceedings of Coastal Dynamics. 029, pp. 36–46.

Castelle, B., Dodet, G., Dodet, G., Scott, T., 2017b. A new climate index controlling winter wave activity along the Atlantic coast of Europe: the West Europe Pressure Anomaly. Geophys. Res. Lett. 44, 1384–1392. https://doi.org/10.1002/2016GL072379.

Castelle, B., Dodet, G., Masselink, G., Scott, T., 2018. Increased winter-mean wave height, variability and periodicity in the North-East Atlantic over 1949-2017. Geophys. Res. Lett. 45, 3586–3596. https://doi.org/10.1002/2017GL076884.

Chadwick, A.J., Karunarathna, H., Gehrels, W.R., Massey, A.C., O'Brien, D., Dales, D., 2005. A new analysis of the Slapton barrier beach system, UK. Proc. Inst. Civ. Eng. Marit. Eng. 158, 147–161. https://doi.org/10.1680/maen.2005.158.4.147.

Clarke, M.L., Rendell, H.M., 2009. The impact of North Atlantic storminess on western European coasts: a review. Quat. Int. 195, 31–41. https://doi.org/10.1016/j.quaint.2008.02.007.

Corbella, S., Stretch, D., 2012. Shoreline recovery from storms on the east coast of South Africa. Nat. Hazards Earth Syst. Sci. 12, 11–22. https://doi.org/10.5194/nhess-12-11-2012.

Davidson, M.A., Splinter, K.D., Turner, I.L., 2013. A simple equilibrium model for predicting shoreline change. Coast. Eng. 73, 191–202. https://doi.org/10.1016/j.coastaleng.2012.11.002.

Dodet, G., Bertin, X., Taborda, R., 2010. Wave climate variability in the North-East Atlantic Ocean over the last six decades. Ocean Model 31, 120–131. https://doi.org/10.1016/j.ocemod.2009.10.010.

Dunstone, N., Smith, D., Scaife, A., Hermanson, L., Eade, R., Robinson, N., Andrews, M., Knight, J., 2016. Skilful predictions of the winter North Atlantic Oscillation one year ahead. Nat. Geosci. 9, 809. https://doi.org/10.1038/ngeo2824.

George, D.A., 2016. Circulation and Sediment Transport at Headlands with Implications for Littoral Cell Boundaries. Unpublished Ph.D. Thesis. University of Southern California.

Goodwin, I.D., Freeman, R., Blackmore, K., 2013. An insight into headland sand bypassing and wave climate variability from shoreface bathymetric change at Byron Bay, New South Wales, Australia. Mar. Geol. 341, 29–45. https://doi.org/10.1016/j.margeo.2013.05.005.

Hails, J.R., 1975a. Some aspects of the quaternary history of Start Bay, Devon. Field Stud. 4 (2), 207–222.

Hails, J.R., 1975b. Submarine geology, sediment distribution and quaternary history of Start Bay, Devon: introduction. J. Geol. Soc. 131, 1–5.

Hails, J.R., 1975c. Offshore morphology and sediment distribution, Start Bay. Philos. Trans. R. Soc. A Math. Phys. Eng. Sci. A 221–228.

Harley, M., 2017. Coastal Storm Definition: Processes and Impacts. https://doi.org/10.1002/9781118937099.ch1.

Harley, M.D., Turner, I.L., Short, A.D., Ranasinghe, R., 2011. A reevaluation of coastal embayment rotation: the dominance of cross-shore versus alongshore sediment transport processes, Collaroy-Narrabeen Beach, southeast Australia. J. Geophys. Res. Earth Surf. 116, 1–16. https://doi.org/10.1029/2011JF001989.

Harley, M.D., Turner, I.L., Short, A.D., 2015. Journal of Geophysical Research: Earth Surface new Insights into Embayed Beach Rotation: the Importance of Wave Exposure and Cross-shore Processes. , pp. 1–15 https://doi.org/10.1002/2014JF003390.

Harley, M.D., Turner, I.L., Kinsela, M.A., Middleton, J.H., Mumford, P.J., Splinter, K.D., Phillips, M.S., Simmons, J.A., Hanslow, D.J., Short, A.D., 2017. Extreme coastal erosion enhanced by anomalous extratropical storm wave direction. Sci. Rep. 7 (6033). https://doi.org/10.1038/s41598-017-05792-1.

Hurrell, James, National Center for Atmospheric Research Staff, 2017. The Climate Data Guide: Hurrell North Atlantic Oscillation (NAO) Index (Station-based). Retrieved from. https://climatedataguide.ucar.edu/climate-data/hurrell-north-atlantic-oscillation-nao-index-station-based.

Kelland, N., 1975. Submarine geology of Start Bay determined by continuous seismic profiling and core sampling. J. Geol. Soc. Lond. 131, 7–17.

Klein, A.H.D.F., Filho, L.B., Schumacher, D.H., 2002. Short-term beach rotation processes in distinct headland bay beach systems. J. Coast. Res. 18, 442–458. https://doi.org/10.2307/4299093.

Lane, S.N., Westaway, R.M., Hicks, Murray D., 2003. Estimation of erosion and deposition volumes in a large, gravel-bed, braided river using synoptic remote sensing. Earth Surf. Process. Landf. 28, 249–271. https://doi.org/10.1002/esp.483.

Lichti, D.D., Gordon, S.J., Tipdecho, T., 2005. Error models and propagation in directly georeferenced terrestrial laser scanner networks. J. Surv. Eng. 131 (4), 135–142.

Mason, T., Bradbury, A., Poate, T., Newman, R., 2009. Nearshore wave climate of the English Channel - evidence for bi-modal seas. Proceedings of International Conference on Coastal Engineering 2008, Hamburg. World Scientific, pp. 605–616.

Masselink, G., Austin, M., Scott, T., Poate, T., Russell, P., 2014. Role of wave forcing, storms and NAO in outer bar dynamics on a high-energy, macro-tidal beach. Geomorphology 226, 76–93. https://doi.org/10.1016/j.geomorph.2014.07.025.

Masselink, G., Scott, T., Poate, T., Russell, P., Davidson, M., Conley, D., 2015. The extreme 2013/2014 winter storms: hydrodynamic forcing and coastal response along the southwest coast of England. Earth Surf. Process. Landf. 41, 378–391. https://doi.org/10.1002/esp.3836.

Masselink, G., Castelle, B., Scott, T., Dodet, G., Suanez, S., Jackson, D., Floc'H, F., 2016. Extreme wave activity during 2013/2014 winter and morphological impacts along the Atlantic coast of Europe. Geophys. Res. Lett. 43, 2135–2143. https://doi.org/10.1002/2015GL067492.

Milan, D.J., Heritage, G.L., Large, A.R.G., Fuller, I.C., 2011. Filtering spatial error from DEMs: Implications for morphological change estimation. Geomorphology 125, 160–171. https://doi.org/10.1016/j.geomorph.2010.09.012.

Morey, C.R., 1976. The natural history of slapton ley nature reserve XII. The morphology and history of the lake basins. Field Stud. 4, 353–368.

Mortlock, T.R., Goodwin, I.D., 2016. Impacts of enhanced central pacific ENSO on wave climate and headland-bay beach morphology. Cont. Shelf Res. 120, 14–25. https://doi.org/10.1016/j.csr.2016.03.007.

Ojeda, E., Guillén, J., 2008. Shoreline dynamics and beach rotation of artificial embayed beaches. Mar. Geol. 253, 51–62. https://doi.org/10.1016/j.margeo.2008.03.010.

Poate, T., Masselink, G., McCall, R.T., Russell, P., Davison, M., 2015. UK storms 2014: gravel beach response. Coastal Sediments 2015. ASCE, San Diego, USA https://doi.org/10.1142/9789814689977_0257.

Poate, T.G., McCall, R.T., Masselink, G., 2016. A new parameterisation for runup on gravel beaches. Coast. Eng. 117, 176–190. https://doi.org/10.1016/j.coastaleng.2016.08.003.

Ranasinghe, R., McLoughlin, R., Short, A., Symonds, G., 2004. The southern oscillation index, wave climate, and beach rotation. Mar. Geol. 204, 273–287. https://doi.org/10.1016/S0025-3227(04)00002-7.

Ruiz de Alegria-Arzaburu, A., Masselink, G., 2010. Storm response and beach rotation on a gravel beach, Slapton Sands, U.K. Mar. Geol. 278, 77–99. https://doi.org/10.1016/j.margeo.2010.09.004.

Santos, V., Haigh, I., Wahl, T., 2017. Spatial and temporal clustering analysis of extreme wave events around the UK coastline. J. Mar. Sci. Eng. 5, 28. https://doi.org/10.3390/jmse5030028.

Scaife, A., Yu Karpechko, A., Baldwin, M., Brookshaw, A., Butler, A., Eade, R., Gordon, M., Maclachlan, C., Martin, N., Dunstone, N., Smith, D., 2015. Seasonal winter forecasts and the stratosphere. Atmos. Sci. Lett. 17, 51–56. https://doi.org/10.1002/asl.598.

Schimel, A.C.G., Ierodiaconou, D., Hulands, L., Kennedy, D.M., 2015. Accounting for uncertainty in volumes of seabed change measured with repeat multibeam sonar surveys. Cont. Shelf Res. 111, 52–68. https://doi.org/10.1016/j.csr.2015.10.019.

Scott, T., Masselink, G., Hare, T.O., Saulter, A., Poate, T., Russell, P., Davidson, M., Conley, D., 2016. The extreme 2013/2014 winter storms: beach recovery along the southwest coast of England. Mar. Geol. 382, 224–241. https://doi.org/10.1016/j.margeo.2016.10.011.

Shaw, J., Duffy, G., Taylor, R.B., Chassé, J., Frobel, D., 2008. Role of a submarine bank in the long-term evolution of the northeast coast of Prince Edward Island. Can. J. Coast Res. 24, 1249–1259. https://doi.org/10.2112/07-08607.1.

Short, A.D., Masselink, G., 1999. Handbook of beach and shoreface morphodynamics. Embayed and Structurally Controlled Beaches. John Wiley.

Sibson, R., 1981. A brief description of natural neighbor interpolation. In: Barnet, V. (Ed.), Interpreting Multivariate Data. Wiley, Chichester, pp. 21–36.

Siggery, E.A., Wiggins, M.A., 2014. Review of the south west coast beach response to wave conditions during the winter of 2013–2014. SouthWest Regional Coastal Monitoring Programme. SW SR01 (Available at). http://www.channelcoast.org/data_management/

online_data_catalogue/metadata/search/index2.php?action=view_metadata&id=408931.
Stockdale, T.N., Molteni, F., Ferranti, L., 2015. Atmospheric initial conditions and the predictability of the Arctic Oscillation. Geophys. Res. Lett. 42, 1173–1179. https://doi.org/10.1002/2014GL062681.
Taylor, J.R., 1997. An Introduction to Error Analysis: The Study of Uncertainties in Physical Measurements. second edition. University Science Books, Sausalito, California.
Thomas, T., Phillips, M.R., Williams, A.T., 2010. Mesoscale evolution of a headland bay: beach rotation process. Geomorphology 123, 129–141. https://doi.org/10.1016/j.geomorph.2010.06.018.
Thomas, T., Phillips, M.R., Williams, A.T., Jenkins, R.E., 2011. Medium timescale beach rotation; gale climate and offshore island influences. Geomorphology 135, 97–107. https://doi.org/10.1016/j.geomorph.2011.08.002.
Thomas, T., Phillips, M.R., Williams, A.T., Jenkins, R.E., 2012. Rotation on two adjacent open coast macrotidal beaches. Appl. Geogr. 35, 363–375. https://doi.org/10.1016/j.apgeog.2012.08.010.
UKHO, United Kingdom Hydrographic Office, 2013. INSPIRE Portal & Bathymetry DAC. Available at. http://aws2.caris.com/ukho/mapViewer/map.action.
van Maanen, B., Nicholls, R.J., French, J.R., Barkwith, A., Bonaldo, D., Burningham, H., Murray, A.B., Payo, A., Sutherland, J., Thornhill, G., Townend, I., van der Wegen, M., Walkden, M.J.A., 2016. Simulating mesoscale coastal evolution for decadal coastal management: a new framework integrating multiple, complementary modelling approaches. Geomorphology 256, 68–80. https://doi.org/10.1016/j.geomorph.2015.10.026.
van Nieuwkoop, J.C.C., Smith, H.C.M., Smith, G.H., Johanning, L., 2013. Wave resource assessment along the Cornish coast (UK) from a 23-year hindcast dataset validated against buoy measurements. Renew. Energy 58, 1–14. https://doi.org/10.1016/j.renene.2013.02.033.
Wang, L., Ting, M., Kushner, P.J., 2017. A robust empirical seasonal prediction of winter NAO and surface climate. Sci. Rep. 7 (279). https://doi.org/10.1038/s41598-017-00353-y.
Westoby, M.J., Brasington, J., Glasser, N.F., Hambrey, M.J., Reynolds, J.M., 2012. 'Structure-from-motion' photogrammetry: a low-cost, effective tool for geoscience applications. Geomorphology 179, 300–314. https://doi.org/10.1016/j.geomorphPH.2012.08.021.
Wheaton, J.M., 2008. Uncertainty in Morphological Sediment Budgeting of Rivers. Unpublished PhD Thesis. University of Southampton (412 pp.).
Wheaton, J.M., Brasington, J., Darby, S.E., Sear, D.A., 2010. Accounting for uncertainty in DEMs from repeat topographic surveys: improved sediment budgets. Earth Surf. Process. Landf. 35, 136–156. https://doi.org/10.1002/esp.1886.
Wiggins, M.A., Scott, T., Masselink, G., Russell, P., Castelle, B., Dodet, G., 2017. The role of multi-decadal climate variability in controlling coastal dynamics: re-interpretation of the "Lost Village of Hallsands". Proceedings Coastal Dynamics 2017. Helsingor, Denmark. 195, pp. 96–107.
Williams, R., 2012. Section 2.3.2: DEMs of difference. In: Cook, S.J., Clarke, L.E., Nield, J.M. (Eds.), Geomorphological Techniques (Online Edition). British Society for Geomorphology, London, UK (ISSN: 2047–0371).
Wolf, J., Woolf, D.K., 2010. Storms and waves. MCCIP Annual Report Card 2010–11; MCCIP Science Review: Suffolk, UK, p. 15.